

1 Interannual variability of the initiation of the phytoplankton 2 growing period in two French coastal ecosystems

3 Coline Poppeschi¹, Guillaume Charria¹, Anne Daniel², Romaric Verney³, Peggy Rimmelin-
4 Maury⁴, Michaël Retho⁵, Eric Goberville⁶, Emilie Grossteffan⁴, Martin Plus²

5 ¹Ifremer, Univ. Brest, CNRS, IRD, Laboratory for Ocean Physics and Satellite remote sensing (LOPS), IUEM,
6 29280 Brest, France.

7 ²Ifremer, DYNECO, Pelagic Ecology Laboratory (PELAGOS), 29280 Brest, France.

8 ³Ifremer, DYNECO, Hydrosedimentary Dynamics Laboratory (DHYSED), 29280 Brest, France.

9 ⁴OSU-European University Institute of the Sea (IUEM), UMS3113, 29280 Plouzané, France.

10 ⁵Ifremer, Morbihan-Pays de Loire Environment Resources Laboratory (LERMPL), 56100 Lorient, France.

11 ⁶Unité Biologie des Organismes et Ecosystèmes Aquatiques (BOREA), Muséum National d'Histoire Naturelle,
12 CNRS, IRD, Sorbonne Université, Université de Caen Normandie, Université des Antilles, Paris, France

13 *Correspondence to:* Coline Poppeschi (coline.poppeschi@ifremer.fr)

14 **Abstract.** Decadal time series of chlorophyll-*a* concentrations sampled at high and low frequencies are explored
15 to study climate-induced impacts on the processes inducing interannual variations in the Initiation of the
16 Phytoplankton Growing Period (IPGP) in early spring. We specifically detail the IPGP in two contrasting coastal
17 temperate ecosystems under the influence of rivers highly rich in nutrients: the Bay of Brest and the Bay of Vilaine.
18 In both coastal ecosystems, we observed a large interannual variation in IPGP influenced by sea temperature, river
19 inputs, light availability (modulated by solar radiation and water turbidity), and turbulent mixing generated by
20 tidal currents, wind stress and river runoff. We show that the IPGP is delayed by around 30 days in 2019 in
21 comparison with 2010. *In situ* observations and a one-dimensional vertical model coupling hydrodynamics,
22 biogeochemistry, and sediment dynamics, show that the IPGP generally not depends on one specific environmental
23 factor, but on the interaction between several environmental factors. In these two bays, we demonstrate that IPGP
24 is mainly caused by sea surface temperature and available light conditions, mostly controlled by the turbidity of
25 the system before first blooms. While both bays are hydrodynamically contrasted, the processes that modulate
26 IPGP are similar. In both bays, IPGP can be delayed by cold spells and flood events at the end of winter, provided
27 that these extreme events last several days.

28 **Keywords**

29 Phytoplankton biomass, Long-term *in situ* observations, Coastal temperate ecosystems, Extreme events, Climate
30 change.
31

32 **1 Introduction**

33 Although studied for 70 years (Sverdrup, 1953), the optimal conditions that trigger the Initiation of
34 Phytoplankton Growing Period (IPGP) in ocean waters in early spring are not well understood (Sathyendranath *et al.*,
35 2015). Three main theories are proposed to date: the Critical Depth Hypothesis (Sverdrup, 1953), the Critical
36 Turbulence Hypothesis (Huisman *et al.*, 1999) and the Disturbance-Recovery Hypothesis (Banse, 1994;
37 Behrenfeld, 2010; Behrenfeld *et al.*, 2013). For Sverdrup (1953), phytoplankton blooms occur when surface mixed
38 layer shoals to a depth shallower than the critical depth, according to light conditions. While Huisman *et al.* (1999)
39 agreed with Sverdrup, he proposed that relaxation of turbulent mixing allows bloom to develop if it occurs below
40 a critical turbulence rate. Behrenfeld (2010) observed blooms in the absence of spring mixed layer shoaling, and
41 declared that the initiation of bloom is controlled by a balance between phytoplankton growth and grazing rate,
42 and suggested a seasonal control of this balance by physical processes. No consensus emerges among these
43 hypotheses – especially because most of these concepts have been defined at specific temporal and spatial scales
44 (Caracciolo *et al.*, 2021; Chiswell *et al.*, 2015) – and the debate is still open, in particular due to the use of more
45 efficient models, the availability of new observations, and the ensuing collection of large *in situ* datasets (Boss and
46 Behrenfeld, 2010; Romyantseva *et al.*, 2019). Coastal waters remain highly dynamic and productive ecosystems
47 at the interface between land and sea, and are distinguished from the waters of the open sea (Gohin *et al.*, 2019;
48 Liu *et al.*, 2019). Because coastal systems are directly influenced by anthropogenic inputs from rivers, no nutrient
49 limitation is observed in late winter. A myriad of factors and mechanisms can then affect the IPGP in coastal areas

(Townsend *et al.*, 1994; Cloern, 1996), but the incident light at the air/sea interface (Glé *et al.*, 2007) and Sea Surface Temperature (SST) (Trombetta *et al.*, 2019) are considered as the main forcings. Low water turbidity also plays an important role, and allows deeper light penetration (Iriarte and Purdie, 2004). This occurs by low vertical mixing conditions in shallow waters (Ianson *et al.*, 2001), *i.e.* limited advective exchanges, weak wind (Tian *et al.*, 2011), neap tide (Ragueneau *et al.*, 1996), and in absence of flooding events (Peierls *et al.*, 2012). Depending on the morphology and hydrodynamics of coastal zones (estuaries, bays, lagoons), the importance of controlling factors can be variable (Cloern, 1996). Temporal variation in IPGP is of great importance in coastal ecosystems because it impacts not only phytoplankton by changing species composition or the succession of species (Ianson *et al.*, 2001; Edwards and Richardson, 2004; Chivers *et al.*, 2020), but also several other biological compartments, such as zooplankton and fish, by species replacements (Sommer *et al.*, 2012).

By amplifying or modifying environmental forcings, it is now well-documented that global climate change may influence the IPGP in coastal areas (Smetacek and Cloern, 2008; Barbosa *et al.*, 2010; Pearl *et al.*, 2014; IPCC, 2021). Heat waves - as opposed to cold spells - have become more frequent in recent years and can advance or delay the IPGP (Gomez and Souissi, 2008). Wind storms, by inducing vertical mixing and sediment resuspension, can have a significant effect on water turbidity, which in turn limits light penetration and therefore influences the IPGP. Floods, following heavier rainfall, may increase continental erosion and ultimately nutrient inputs to coastal ecosystems. Because coastal ecosystems are strongly influenced by human activities such as changes in land use, quantifying the contribution related to long-term climate-induced signals is challenging (Krompkamp and Van Engeland, 2010).

Our study is based on two geographically close, but hydrodynamically different, nearshore ecosystems: (1) the Bay of Brest, a shallow semi-enclosed bay with well-mixed waters (Le Pape and Menesguen, 1997) and (2) the Bay of Vilaine, a shallow open bay with long water residence times (Chapelle *et al.*, 1994). These two coastal ecosystems are strongly impacted by anthropogenic pressures, such as intensive agriculture (Ragueneau *et al.*, 2018; Ratmaya *et al.*, 2019), which induces highly rich nutrient waters.

In this study, we aim to better understand interannual local changes in the IPGP in coastal temperate ecosystems in the current context of global climate change over the last 20 years. As most studies dealing with IPGP are mainly based on discrete water sampling (Iriarte *et al.*, 2004; Tian *et al.*, 2011) or modeling (Townsend *et al.*, 1994; Philippart *et al.*, 2010), we focus here on the use of long-term high-frequency observations to assess interannual variability of the IPGP, and to identify the triggering and controlling factors. We detect and analyze the temporal variability of the IPGP and quantify how environmental forcings influence its dynamics. To detect and analyze IPGP in coastal environments, we develop a numerical framework that combines high-frequency decadal *in situ* observations and a one-dimensional vertical (1DV) hydro-sedimentary and biogeochemical coupled numerical model. The potential impact of hydro-meteorological extreme events, such as cold spells, flood events and wind bursts, on the IPGP is then investigated.

2 Data and methods

2.1 Study areas

Our study focuses on two northwestern French coastal temperate ecosystems located in the Bay of Biscay, the Bay of Brest and the Bay of Vilaine, two ecosystems impacted by excessive nutrient inputs from watersheds, but exposed to different hydrodynamic conditions.

The Bay of Biscay is a region with a complex system of coastal currents influenced by the combined effects of seasonal wind regimes and important river discharges modulated by large-scale gyre circulation patterns (Ferrer *et al.*, 2009; Lazure and Jégou, 1998; Lazure *et al.*, 2006; Isemer and Hasse, 1985; Pingree and Le Cann, 1989, 1990; Le Boyer *et al.*, 2013; Lazure *et al.*, 2006; Charria *et al.*, 2013). In the Iroise Sea, at spring tide close to the islands and capes, tidal currents can reach 4 m s^{-1} (Muller *et al.*, 2010). This tidal circulation combined with meteorological forcings and sharp thermal gradients generate a strongly variable local circulation. In the vicinity of the Loire estuary, the freshwater discharges in the surface layers induce important density gradients driving a poleward circulation (about 10 cm s^{-1}) modulated by wind forcings (Lazure and Jégou, 1998; Lazure *et al.*, 2006). The river plumes can propagate under specific conditions towards the South-West.

Under these hydrodynamic conditions, the Bay of Brest is a semi-enclosed bay (180 km^2) with 50% of the surface shallower than 5 m depth. The Bay is connected with the Atlantic Ocean (Iroise sea) through a narrow

110 and shallow strait. Tidal variation reaches 8 m during spring tides, which represents an oscillating volume of 40%
111 of the high tide volume. Freshwater inputs come from the Aulne river (catchment area 1875 km², mean river flow
112 26 m³ s⁻¹), and two smaller rivers, the Elorn (catchment area 385 km², mean river flow 6 m³ s⁻¹) and the Mignonne
113 (catchment area 111 km², mean river flow 1.5 m³ s⁻¹). Due to the macrotidal regime, associated with a strong
114 vertical mixing, the high nitrate concentrations do not generate important green tides (Le Pape *et al.*, 1997). Strong
115 decreases in the Si:N and Si:P ratios did not exhibit dramatic phytoplankton community shifts from diatoms to
116 non-siliceous species in spring (Del Amo *et al.*, 1997), because of the high Si recycling (Ragueneau *et al.*, 2002;
117 Beucher *et al.*, 2004).

118
119 The Bay of Vilaine is a mesotidal open bay (69 km²) under the influence of the Vilaine (catchment area
120 10 500 km², mean river flow 70 m³ s⁻¹) and the Loire (catchment area 117 000 km², mean river flow 850 m³ s⁻¹)
121 river discharges, with tidal ranges varying between 4 and 6 m (Merceron, 1985). The Loire river plume tends to
122 spread northwestward, with a dilution of 20- to 100-fold by the time it reaches the Bay of Vilaine (Ménesguen *et al.*,
123 2018). The Vilaine river plume tends to spread throughout the bay before moving westward (Chapelle *et al.*,
124 1994). The water residence time varies seasonally between 10 and 20 days (Chapelle *et al.*, 1994). The water
125 circulation is mainly driven by tides, winds and river flows (Lazure and Jegou, 1998). This bay is well known as
126 one of the most sensitive European Atlantic coastal ecosystems to eutrophication (Ménesguen *et al.*, 2019). The
127 Bay of Vilaine has undergone eutrophication over recent decades mainly due to high nutrient inputs from the
128 Vilaine and Loire rivers (Rossignol-Strick, 1985; Ratmaya *et al.*, 2019).

129 2.2 *In situ* observations

130
131 COAST-HF-Iroise (Rimmelin-Maury *et al.*, 2020) and COAST-HF-Molit (Retho *et al.*, 2020) are two high-
132 frequency monitoring buoys of the French national observation network COAST-HF¹ (Répécaud *et al.*, 2019;
133 Farcy *et al.*, 2019; Cocquempot *et al.*, 2019; Poppeschi *et al.*, 2021) located respectively in the Bay of Brest
134 (4.582°W; 48.357°N) and in the Bay of Vilaine (2.660°W; 47.434°N) (Fig. 1). COAST-HF-Iroise has been
135 operating in the strait between the Bay of Brest and the Iroise sea since 2000. COAST-HF-Molit buoy has been
136 sampling the plume of the Vilaine river since 2008. Buoys are deployed during the whole year except for COAST-
137 HF-Molit that is only available for part of the year prior to 2018 (from mid-February to early September, i.e. from
138 day 50 to 250 for the period 2008-2017). Depending on the tide, the depth at the mooring sites ranges from 11 to
139 17 m for both COAST-HF buoys. Environmental parameters (SST, salinity, turbidity, dissolved oxygen and Chl-
140 *a* fluorescence) are measured at 1 to 2 m below the surface every 20 minutes (COAST-HF-Iroise) or every hour
141 (COAST-HF-Molit). The Chl-*a* fluorescence, a proxy of phytoplankton biomass (FFU unit), is measured by a
142 Turner CYCLOPS-7 Sensor (precision \pm 5%).

143 Sub-surface Chl-*a* concentrations are provided by two French marine monitoring networks, the SOMLIT
144 coastal observation network² and the REPHY (French Observation and Monitoring program for Phytoplankton
145 and Hydrology in coastal waters)³. Samples are collected bimonthly at the SOMLIT-Brest (4.552°W; 48.358°N)
146 and the REPHY-Loscolo (2.445°W; 47.496°N) stations, which are close to the COAST-HF stations. Chl-*a*
147 concentrations are measured with either spectrophotometric or fluorimetric methods (Aminot and K erouel, 2004).
148

149 Daily river flows are measured at gauging stations (French hydrology “Banque Hydro” database⁴), located
150 close to the main river mouths [Aulne-Gouezec (4.093°W; 48.205°N), Loire-Montjean (1.78°W; 47.106°N)]. The
151 Vilaine river flow is controlled by a dam, and data are provided by the Vilaine Public Territorial Basin
152 Organization⁵ (Fig. 1).
153

154 The tide gauge stations (Shom⁷) at Brest (4.495°W; 48.382°N) and Crouesty (2.895°W; 47.542°N) record the
155 sea level every minute.
156

¹ www.coast-hf.fr, data available on www.coriolis-cotier.org

² <https://somlit.fr>

³ <https://doi.org/10.17882/47428>

⁴ www.hydro.eaufrance.fr/

⁵ <https://www.eptb-vilaine.fr/>

⁶ <https://donneespubliques.meteofrance.fr/>

⁷ <http://data.shom.fr>

157 Precipitation, air temperature, wind direction and intensity, and the solar flux data are retrieved every 6 minutes
158 from two meteorological stations from the Météo-France observation network⁶: Guipavas (4.410°W; 48.440°N)
159 and Vannes-Séné (2.425°W; 47.362°N) (Fig. 1). We use the solar flux as a proxy for subsurface PAR
160 (Photosynthetically Available Radiation).

161 2.3 MARS3D-1DV modeling experiments

162 2.3.1 MARS3D-1DV model

163
164 A 1DV (one-dimensional vertical) model configuration is implemented to simulate changes in biogeochemical
165 variables due to hydrodynamics and sediment dynamics in both bays.
166

167 The hydrodynamical model is based on the code developed for MARS3D (3D hydrodynamics Model for
168 Applications at Regional Scale; Lazure and Dumas, 2008). This model is a primitive equation model with a free
169 surface and uses the Boussinesq and hydrostatic pressure assumptions. We use the 1DV configuration of the
170 model, with 10 vertical sigma levels for 15 m depth and a time step of 30s.
171

172 The sediment model (MUSTANG - Le Hir *et al.*, 2011; Grasso *et al.*, 2015; Mengual *et al.*, 2017) is designed
173 to simulate the transport and changes in different sediment mixtures. In the sediment, 50 layers (refined near the
174 surface) for a total thickness of 40 cm are implemented. Four sediment classes are considered: muds (diameter 10
175 μm), fine sand (diameter 100 μm), medium sand (diameter 200 μm) and coarse sand (diameter 400 μm). The
176 sediment dynamics (transport in the water column, exchanges at the water/sediment interface, erosion/deposition
177 processes) are driven by an advection/dispersion equation for each sediment class (refer to Le Hir *et al.*, 2011 for
178 a detailed description of the sediment model).
179

180 The biogeochemical model BLOOM (Biogeochemical Coastal Ocean Model) is derived from the ECO-
181 MARS model (Cugier *et al.*, 2005; Ménesguen *et al.*, 2019) adding major processes of early diagenesis. Nitrogen,
182 phosphorus, and silica cycles are studied considering four nutrients: nitrate, ammonium, soluble reactive
183 phosphorus and silicic acid (sorption/desorption of phosphate on suspended sediment and precipitation/dissolution
184 of phosphate with iron processes are also included). The model is also represented by three phytoplankton classes
185 (microphytoplankton, dinoflagellates, pico-nano-phytoplankton), two zooplankton classes (micro- and meso-
186 zooplankton), and exchanges at the water/sediment interface and inside the sediment compartment.

187 2.3.2 MARS3D-1DV model sensitivity experiments

188
189 These three models (hydrodynamical, sediment and biogeochemical) are coupled online during simulations
190 and allow the nutrient and phytoplankton dynamics in both bays to be reproduced. The simulation for the Bay of
191 Brest does not include nutrient inputs from the sediment because it is considered to be negligible around the
192 COAST-HF-Iroise station.
193

194 Dissolved and particulate variables are defined in the water column and in the sediment. Initial values for both
195 bays are uniform over the initial vertical profile (Table 1) and are based on a 3D realistic coupled simulation during
196 the year 2015. Values for the 15th of February are extracted at the position of COAST-HF-Iroise for the Bay of
197 Brest and at the position of COAST-HF-Molit station for the Bay of Vilaine (Plus *et al.*, 2021).
198

199 To evaluate the sensitivity of the biogeochemical dynamics to environmental conditions, sensitivity
200 experiments are then performed using the coupled MARS3D/BLOOM/MUSTANG 1DV model configuration. All
201 simulations are started at the end of winter (15th February) and run until the end of the year. The range of values
202 used in the sensitivity experiments are derived from the minimum and maximum observed *in situ* data. Each
203 parameter is tested with a constant value for the whole simulation.
204

205 Three parameters are individually explored in both bays:

- 206 - The air temperature in sensitivity experiments ranges from 4 to 14°C and is controlled by the intensity of
207 solar radiations. Air temperature represents the main controlling parameter of SST in the 1DV model. This
208 parameter drives the radiative fluxes in the model and then constrains SST.
- 209 - Wind intensity effect on the IPGP is explored for values between 0 and 10 m s⁻¹. In the 1DV model, wind
210 is a source of vertical mixing in the simulation.

211 - The Cloud Coverage (CC) sensitivity experiments ranged in value between 0 and 100% CC. This
212 parameter is a driver of Photosynthetic Available Radiation (PAR) in the ocean. For the formulation of
213 radiative fluxes in the 1DV MARS3D model, 100% cloud coverage allows an inflow of 38% of the total
214 solar radiation in the water column. Each individual experiment is associated with a constant CC applied
215 to the seasonal solar radiation.
216

217 In the Bay of Vilaine, the sediment plays a role on light penetration and acts as an active source of nutrients: we
218 therefore explored the influence of mud erosion rate (values between $2 \cdot 10^{-5}$ and $2 \cdot 10^{-7}$ $\text{kg m}^{-2} \text{s}^{-1}$) in that bay (sand
219 erosion rate fixed to $0.0001 \text{ kg m}^{-2} \text{s}^{-1}$). For the sensitivity experiments, it drives a mass of sediment eroded and
220 resuspended and a bottom input of nutrients in the water column.
221

222 A second set of experiments is conducted by combining the individual effect of environmental parameters in order
223 to explore possible cumulative or opposite effects on the IPGP. The upper and lower bounds of the range of
224 environmental parameters are taken into account. Experiments are detailed in Table 5.

225 **2.4 Data processing**

226 **2.4.1 Chl-*a* fluorescence data**

227
228 To analyze high-frequency time series of *in situ* Chl-*a* fluorescence, the Quenching effect (Lehmuskero
229 *et al.*, 2018) - a decrease in fluorescence in the presence of light (Fig. 2) - is removed by analyzing only night-time
230 data, as reported in Carberry *et al.* (2019). Chl-*a* fluorescence data are studied on a daily basis, i.e. averaged from
231 10 pm to 5 am. Years with less than 75% of valid data are not considered in our analyses: for the Bay of Brest,
232 2005, 2006, 2008, 2009 and 2018.

233 **2.4.2 Detection of the IPGP**

234
235 On the basis of literature, we first apply three methods to determine the annual IPGP dates:
236 - (1) Set an arbitrary beginning and end of the phytoplankton growing period at 20% and 80% of the
237 cumulative Chl-*a* fluorescence measured from January 1st to December 31st (Kromkamp *et al.*, 2010).
238 - (2) Consider a threshold of 5% above the yearly median chlorophyll (Brody *et al.*, 2013).
239 - (3) Consider the beginning of the growing period as the maximum daily difference in Chl-*a* fluorescence
240 (Philippart *et al.*, 2010).
241

242 Because none of these methods allowed us to obtain a valid IPGP detection - with a too late (method 1)
243 or a too early (method 2) detection, or multiple IPGP dates (method 3) - we elaborate a detection method based on
244 discontinuities of the Chl-*a* fluorescence signal (Fig. 3): daily FFU slopes are calculated based on a linear
245 regression over a ± 2 day window for each day, from 1st January to 31st December, and each year. The IPGP date
246 is identified when the slope exceeds a threshold value - defined as the median of the daily slopes - for the first time
247 in the year for at least 20 days. The end of the phytoplankton growing period is determined when the slope
248 stabilizes below the threshold for at least 20 days for the last time in the year. The cumulative Chl-*a* fluorescence
249 corresponds to the duration of the growing period.

250 **2.4.3 Pattern of the phytoplankton growing period**

251
252 The k-means method (Hartigan and Wong, 1979) is used to characterize the annual patterns of the
253 phytoplankton growing period.

254 We exclude the year 2013 from the analysis of the Bay of Vilaine because of a large number of missing
255 data. When the interval over which consecutive data are missing is no longer than one week, we perform a linear
256 interpolation to replace the missing data. A 5-day running average is applied to the Chl-*a* fluorescence signal and
257 data are then normalized by the maximum value. We analyze Chl-*a* fluorescence every year for 150 days after the
258 IPGP.

259 Time series from both bays are merged before application of the k-means and the number of clusters (or
260 centroids) is set at 2 to distinguish the dominant patterns of the phytoplankton growth period at both sites. The use
261 of a larger number of clusters is investigated and does not produce a pattern representing a large number of
262 observed growing periods.

263 2.4.4 Detection of extreme events

264
265
266
267
268
269
270
271
272

The peak over threshold method (see Oliver *et al.*, 2018 and Poppeschi *et al.*, 2021 for further details) is used to detect hydro-meteorological extreme events such as cold spells, flood events and wind bursts. An event is considered as extreme if values are higher than a given statistical threshold for at least 3 consecutive days. In the present study, the 90-percentile threshold is selected to detect floods and wind bursts, and the 10-percentile to detect cold spells. Seasonal anomalies are calculated over at least 20 years, by subtracting raw data from the winter average value (for cold spells) or from the spring average value (wind bursts and floods).

273 3. Results

274 3.1 Characterization of the phytoplankton growing period

275
276
277
278
279
280
281
282
283
284
285
286

The high-frequency *Chl-a* fluorescence time series at both sites show an intense seasonal cycle with low values from November to February and high values from March to October (Fig. 4). Focusing on the period from 2010 to 2019 in the Bay of Brest, the minimum *Chl-a* fluorescence is observed during the years 2012 and 2013 and does not exceed 7 FFU. In contrast, some years show *Chl-a* fluorescence values above 15 FFU, but can be up to 20 FFU (such as 2010, 2014, 2015 or 2019). In the Bay of Vilaine, a similar seasonal pattern is observed with higher values reaching 50 FFU in 2013. Small (< 20 FFU) and high (> 35 FFU) *Chl-a* fluorescence amplitude are observed occasionally (in 2014 and 2017 and in 2013 and 2016, respectively). The *Chl-a* fluorescence is higher, almost double, in the Bay of Vilaine compared to the Bay of Brest with a mean cumulative *Chl-a* fluorescence around 580 FFU and 360 FFU, respectively (Table 2). The high phytoplankton biomass of the Bay of Vilaine is corroborated by the concentrations measured by low-frequency observation programs (SOMLIT and REPHY).

287
288
289
290

The phytoplankton growing period ranges from approximately March 10th to September 30th in both regions (Table 2). The average duration of the phytoplankton growing period is 179 days in the Bay of Vilaine and 200 days in the Bay of Brest (Table 2). The phytoplankton growing period is characterized by successive blooms, whose number and intensity are variable from year to year (Fig. 4).

291
292
293
294
295
296
297
298

The main patterns of the phytoplankton growing period are identified by two clusters (Fig. 5). Cluster 0 includes the phytoplankton growing period with two successive marked blooms in early spring and in summer, the intensity of the second bloom being highly variable. Cluster 1 is characterized by a plateau during the two first months of the phytoplankton growing period. Most of the patterns of the Bay of Vilaine are in cluster 0 while those of the Bay of Brest are in cluster 1 (Table 3). The years that stand out in the Bay of Brest (2002, 2010, 2014) correspond to years with the highest cumulative *Chl-a* fluorescence (≥ 450 FFU). The atypical years in the Bay of Vilaine (2011, 2017 and 2019) show the lowest cumulative *Chl-a* fluorescence (≤ 450 FFU).

299 3.2 Variability of the Initiation of the Phytoplankton Growing Period (IPGP)

300
301
302
303
304
305
306

Calculations performed to determine the IPGP for high- and low-frequency data yield comparable results (Fig. 6). The mean differences between the IPGP calculated with the high- and low-frequency data are 5 and 8 days for the Bay of Brest and the Bay of Vilaine, respectively. A difference of only 4 and 6 days between the model simulations (reference year = 2015) and the high-frequency *in situ* data is observed in the Bay of Brest and the Bay of Vilaine, respectively.

307
308
309
310
311

A decadal variability of the IPGP is recorded from mid-February to mid-April in both ecosystems (day 50 to day 102 in the Bay of Brest and day 53 to day 93 in the Bay of Vilaine; Fig. 6). In the Bay of Brest, early IPGPs (day < 53) are observed in 2010 and 2013, whereas late IPGP (day > 93) are observed in 2001, 2017 and 2019. In the Bay of Vilaine, the earliest IPGP is detected in 2012 (day 53) and the latest in 2019 (day 93).

312
313
314
315

The variability of IPGP in the Bay of Brest shows two linear trends (Fig. 6a), with a decrease of 52 days from 2001 to 2010 (observed in both high- and low-frequency datasets), followed by an increase (+48 days) from 2011 to 2019, a decline also observed in the Bay of Vilaine (Fig. 6b). Over the period 2011-2019, the IPGP is shifted towards a later date by +3.5 days per year in the Bay of Vilaine and +3.7 days per year in the Bay of Brest.

316 3.3 Analysis of environmental conditions driving the IPGP

317 3.3.1 Impact of environmental conditions on the IPGP

318
319
320
321
322

We next quantify the influence of environmental drivers on the date of IPGP (Fig. 7). These drivers represent the major limiting factors of the phytoplankton growth and comprise input of nutrients (river flow), PAR (incident light), SST (air temperature, incident light) and turbidity in the water column (river flow, wind intensity, tidal range).

323
324
325
326
327
328
329

The median values of the environmental drivers observed at the date of each annual IPGP are very close in both bays (Table 4): temperate SST (10 °C), weak wind (3 m s⁻¹), a medium PAR (1360 W m⁻²), a low turbidity (7 NTU), and a weak tidal amplitude (semi-amplitude of 1.6 m in the Bay of Brest and 0.9 m in the Bay of Vilaine). The IPGP occurs mainly during neap tides at 68% in the Bay of Brest and 77% in the Bay of Vilaine. The river flow is low during the IPGP with a runoff of 46 m³ s⁻¹ for the Aulne, 96 m³ s⁻¹ for the Vilaine, and 1196 m³ s⁻¹ for the Loire. These values are considered to be the favorable environmental conditions for this study.

330
331
332
333
334

To assess how environmental drivers may impact (i.e. advance or delay) the IPGP, we focus on the 15 days before the mean day of the IPGP (day 68) and of each annual IPGP. The considered 15 days length is related to the typical water residence time in both bays (Frere *et al.*, 2017; Poppeschi *et al.*, 2021 for the Bay of Brest - Chapelle *et al.*, 1994; Ratmaya *et al.*, 2019 for the Bay of Vilaine).

335
336
337
338
339
340

The earliest IPGP dates (IPGP < day 55) are associated with earlier occurrence of favorable environmental conditions than the other years. Earliest IPGP in 2010 and 2013 in the Bay of Brest and in 2012 in the Bay of Vilaine occurred before day 55 (Fig. S1f, 7c - S2a). Early IPGP between day 55 to 60, also associated with favorable environmental conditions, are found in 2002 and 2016 in the Bay of Brest (Fig. S1b, S1j).

341
342
343
344
345
346
347

The latest IPGP dates (IPGP > day 90) are associated with unfavorable environmental conditions until the date of the IPGP. Latest IPGP occurring after day 90 are observed in 2001, 2003, 2017 and 2019 in the Bay of Brest and in 2019 in the Bay of Vilaine (Fig. S1a,c,k,l - S2g). For example, the delay detected in 2017 in both bays is due to strong wind and a lack of PAR until the day of IPGP (Fig. S1k - Fig. S2e). Late IPGP between day 70 to 90 are recorded in 2004, 2007 and 2012 in the Bay of Brest, and in 2014, 2017 and 2018 in the Bay of Vilaine (Fig. S1d,e,g, 7d - S2e,f).

348
349
350
351
352
353

The interannual variability of the date of the IPGP is therefore not controlled by a unique environmental driver. When the values of the environmental drivers responsible for the IPGP (Table 4) are compared to the mean values of the environmental drivers over a period of 30 days around the IPGP (Table S1), threshold values are observed in both bays: river flow is lower than usual (between 10 and 30 m³ s⁻¹), temperature is close to the expected value (10 °C), wind is weak (0.5 to 1.5 m s⁻¹), PAR is stronger (>300 W m⁻²), and turbidity is low (about 1.5 NTU). IPGP starts around day 68 (±3 days) on average (Fig. 7a,b).

354 3.3.2 Modeling the importance of the environmental drivers

355
356
357

The relative contribution of each environmental driver on the IPGP is determined by MARS-1DV simulations starting on February 1st (Fig. 8). Environmental drivers tested in the model are controlling:

358
359
360
361

- sea temperature - explored in the model through air temperature (SST proxy),
- the level of water turbulence - through wind intensity,
- the available light - controlled by Cloud Coverage (CC, as a sea surface PAR proxy) and the erosion rate (turbidity proxy) limiting light penetration in the water column.

362
363
364
365
366
367

Model results show that early IPGP are associated with air temperature higher than 9 °C (resulting in SST higher than 8 °C), low wind intensity, weak CC and low erosion rate. Environmental drivers responsible for early or late IPGP are similar in both bays. Air temperature is the main driver with a potential deviation from the mean IPGP of 25 days in the Bay of Brest and 40 days in the Bay of Vilaine (Fig. 8). Wind, CC and erosion rate have a lower impact on the IPGP (around 6 days in the Bay of Brest and 13 days in the Bay of Vilaine). In the Bay of Vilaine, the environmental drivers can simulate later IPGP than in the Bay of Brest.

368 In the Bay of Brest (Fig. 8a), only variations in air temperature have a real impact on the IPGP. If air
369 temperature is low ($< 8^{\circ}\text{C}$), the IPGP is not triggered before day 74 (Table 5, Exp 1). If air temperature is high
370 ($>13^{\circ}\text{C}$), the IPGP can start on day 49 (Table 5, Exp 2).

371
372 In the Bay of Vilaine, air temperature and the erosion rate are the two main drivers impacting the IPGP (Fig.
373 8b). As in the Bay of Brest, if air temperature is low ($< 6^{\circ}\text{C}$), the IPGP is late and appears only after day 80 (Table
374 5, Exp 1). If temperature is equal or above 13°C , the IPGP is early and appears on day 45 (Table 5, Exp 2). If the
375 erosion rate is low ($2 \cdot 10^{-7} \text{ kg m}^{-2} \text{ s}^{-1}$), the IPGP takes place on day 76 (Table 5, Exp 7). If the erosion rate is high
376 ($2 \cdot 10^{-5} \text{ kg m}^{-2} \text{ s}^{-1}$), the IPGP occurs late after day 87 (Table 5, Exp 8).

377
378 Even if variations in wind and CC induce weaker shifts in the date of the IPGP, i.e. about one week at the
379 most (Table 5, Exp 3,4,5,6), they can however explain some variations in IPGP. For example, the fact that the
380 early IPGPs, observed in 2010 in the Bay of Brest and in 2012 in the Bay of Vilaine, are due to low wind conditions
381 (around 2 m s^{-1} , Fig. S2a - S1f) are confirmed by both *in situ* measurements and the model (Fig. 8b).

382
383 The combined effect of the environmental factors can also be explored from the MARS-1DV model
384 simulations (Fig. 9). The modeling conditions (hereafter called “Exp”) are detailed in Table 5 and compared to the
385 mean IPGP date (day 68).

386
387 The simulations confirm the observations, late IPGP correspond to the most extreme unfavorable
388 combined environmental values (temperature of 4°C , wind intensity of 10 m s^{-1} , CC of 100% and erosion rate of
389 $2 \cdot 10^{-5} \text{ kg m}^{-2} \text{ s}^{-1}$ - Exp A). Due to the most unfavorable conditions, the IPGP occurs 9 days and 64 days later in the
390 Bay of Brest and in the Bay of Vilaine, respectively. Late IPGP can also be linked to the combined effect of only
391 two factors such as: “temperature and wind” and “temperature and CC” with a delay of 5 and around 22 days
392 respectively (Exp B and C). In contrast, no delay is observed for the combination “wind and CC” (Exp D) in both
393 bays.

394
395 Early IPGP events are found in the model simulations and in the *in situ* observations when conditions
396 correspond to a high temperature (14°C), no wind intensity and CC, and a low erosion rate ($2 \cdot 10^{-7} \text{ kg m}^{-2} \text{ s}^{-1}$) -
397 Exp K. All the combined scenarios allow the occurrence of an earlier IPGP (by at least 5 additional days) compared
398 to experiments that consider a single modified parameter.

399
400 This analysis enables environmental parameters to be classified with respect to their impact on the IPGP.
401 In both bays, the temperature appears to be the key factor driving the IPGP. By combining the environmental
402 drivers, the IPGP can occur even later or earlier than with a single forcing. In both bays, the combination of wind
403 and CC has no impact on the IPGP, which occurs near the median day (Exp D and N). The extreme couplings of
404 Exp A,E,F,G,J delay the date of IPGP later than detected in the observations for the Bay of Vilaine. All simulations
405 show a higher impact on the date of IPGP in the Bay of Vilaine than in the Bay of Brest (Fig. 9, Table 5).

406 3.4 Impact of extreme hydro-meteorological events on the IPGP

407 3.4.1 Cold spells

408 The impact of cold spells on the IPGP is simulated with the MARS-1DV model based on two criteria: (i)
409 the period of occurrence of the event, set in mid- or end February, (ii) the duration and intensity of the cold spell,
410 which can be either short and weak (8 days, 7°C) or long and intense (20 days, 5°C) (Fig. 10).

411 In both bays, when the cold spell appears in mid-February, the IPGP is not impacted. However, it is
412 delayed by about 15 days when occurring at the end of February. The duration of the cold spell, when longer than
413 15 days, also has an impact on the IPGP, with a delay of 13 and 12 days in the Bay of Brest and in the Bay of
414 Vilaine, respectively.

415 Eight cold spells are detected in February in both bays between 2001 and 2019. In 2011, both sites are
416 impacted simultaneously with cold spells. Long cold spells (30 days) are observed in 2009 and 2018, leading to
417 an anomaly of more than -1.9°C .

418 The cold spell observed in 2018 in the Bay of Vilaine may explain the later IPGP. There is no change in
419 the IPGP in 2011 and 2013, despite the cold spell, the period of occurrence being too early during winter 2011,
420 and the duration too short in 2013 (only 10 days).

421 In the Bay of Brest, the cold spells in 2003 and 2004 may explain the delay of the IPGP (respectively
422 days 93 and 85). The presence of long and intense cold spells in 2010 and 2011 do not shift the IPGP (days 50 and
423 67) because they occur too early (before day 20).

424 3.4.2 Wind bursts

425 Based on our model simulations, the wind bursts that occur during at least three continuous days have no
426 impact on the IPGP in both bays, whatever the duration, the period and the intensity (± 1 day). In the Bay of
427 Vilaine, only one wind event is detected in 2018 (3 days long and 6 m s^{-1}). In the Bay of Brest, several events are
428 detected, but no significant impact is observed on the IPGP.
429
430

431 3.4.3 Flood events

432 River floods can delay the IPGP by resuspending sediment in the water column and therefore limiting
433 light penetration in the water column. Inputs of nutrients have no impact during the late winter period because
434 nutrient concentrations are maximal, with no limitation on phytoplankton growth. Flood events are analyzed with
435 observation data collected in the month prior to the IPGP date because the 1DV modeling approach does not allow
436 the sensitivity to hydrological events to be simulated (*i.e.* it is necessary to simulate horizontal advection
437 processes).
438

439
440 In the Bay of Brest, the impact of flood events depends on their duration and intensity: when the flood
441 exceeds 15 days, a delay in the IPGP is detected. Shorter and more intense floods ($> 300 \text{ m}^3 \text{ s}^{-1}$) do not impact the
442 IPGP.
443

444 In the Bay of Vilaine, only two flood events are observed close to the IPGP date in 2014 and 2015. The
445 2015 flood event, which is 10 days longer and more intense ($> 100 \text{ m}^3 \text{ s}^{-1}$) than the 2014 one, delays the IPGP date
446 by 10 days.
447

448 4 Discussion

449 4.1 Comparison of the phytoplankton growing period in both bays

450
451 Despite their contrasting hydrodynamics (*e.g.* Petton *et al.*, 2020; Poppeschi *et al.*, 2021; Lazure and
452 Jegou, 1998; Ratmaya *et al.*, 2019; Menesguen *et al.*, 2019), the median dates of the start and the end of the
453 phytoplankton growing period are the same in the Bay of Brest and in the Bay of Vilaine, whether they are
454 calculated from high- and low- frequency datasets or model simulations. The phytoplankton growing period occurs
455 from March to September and lasts about 190 days in both bays. This concordance is related to a similar seasonality
456 of the environmental drivers.
457

458
459 The observed cumulative fluorescence is almost double in the Bay of Vilaine compared with the Bay of
460 Brest. This difference in the amount of chlorophyll produced in surface waters from both bays is also recorded by
461 the low-frequency observation programs and satellite observations (Menesguen *et al.*, 2019). It can be explained
462 by the difference of the hydrodynamics and the influence of different watersheds. The Bay of Brest is a semi-
463 enclosed bay with a macro-tidal regime influenced by two local rivers (Aulne and Elorn), whereas the Bay of
464 Vilaine has a weaker tidal regime, is open on the continental shelf and is widely influenced by a large river (Loire
465 river).
466

467 Two different patterns of the phytoplankton growing period are identified by the k-means classification
468 in both bays. The flattened, weak and long bloom highlighted in the Bay of Brest can be explained by assuming
469 that nutrients are not limiting the phytoplankton growth during spring. The maintenance of the diatom succession
470 throughout spring since the 1980s (Quéguiner 1982; Del Amo *et al.*, 1997) can be explained by the combination
471 of increasing N and P loads, intense Si recycling and a macrotidal regime (Ragueneau *et al.*, 2019). The
472 phytoplankton growing period in the Bay of Vilaine is characterized by several successive peaks including two
473 main ones. Nutrients drive the seasonal evolution of the phytoplankton growing period through periods of nutrient-
474 limited conditions. These fluctuations are governed by phosphorus and nitrate loads from Vilaine and Loire rivers

475 (Ratmaya *et al.*, 2019), but probably also by the stoichiometry of recycled elements in the water and at the water-
476 sediment interface (Ratmaya *et al.*, 2022). At the beginning of the phytoplankton growing period (IPGP), however,
477 the system is not nutrient-limited in terms of nitrate, phosphorus and silicate (Table 4).
478

479 4.2 Validation of the method for IPGP detection

480

481 The method that we developed to detect IPGP on both high-frequency and low-frequency *in situ*
482 observations shows comparable results and detects similar initiation dates for some years, while a time lag between
483 high- and low-frequency observations can be observed for other years. This difference is mainly explained by the
484 difference in the sampling frequency. The late deployment of the buoy in the Bay of Vilaine (i.e. not deployed
485 until mid-February before 2018) can also explain some differences between both sites. High-frequency data
486 provide a more accurate detection of the day of the IPGP, while an uncertainty of about ± 7 days is observed with
487 low-frequency observations. This comparison between high- and low-frequency based IPGP detection highlights
488 the sensitivity of sampling strategy in the observation of phytoplankton growing periods (Bouman *et al.*, 2005;
489 Serre-Fredj *et al.*, 2021) related to the response of the ecosystem within a few hours after an environmental change
490 (Lefort and Gasol, 2014; Thyssen *et al.*, 2008).
491

492 The modeled IPGP, based on the year 2015, is coherent with high-frequency observations (around 5 days
493 of difference between modeled and observed IPGP). Considering the idealized framework for modeling
494 computations (1DV model instead of a realistic 3D model configuration), the agreement between observations and
495 simulations validates the 1DV approach to explore IPGP dynamics. With the 1DV configuration, the vertical
496 dynamics in the water column, coupled with biogeochemistry and sediment dynamics are well reproduced.
497 Atmospheric forcings and interactions with the bottom layer are the main environmental drivers. The full range of
498 impacts related to the horizontal advection (*e.g.* in considered regions, rivers advected plumes can change the
499 hydrodynamics and the nutrient fluxes) are not evaluated, however. In the Bay of Brest and in the Bay of Vilaine,
500 such advected sources exist (Poppeschi *et al.*, 2021; Lazure and Jegou, 1998). But inputs from rivers are not main
501 drivers of the IPGP in nutrient-rich environments. Nutrient loads advected by rivers may impact the phytoplankton
502 community later during the growing period rather than at IPGP (Ratmaya *et al.*, 2019).
503

504 4.3 Identification of the environmental conditions supporting the IPGP

505

506 The main theories to explain the initiation of phytoplankton blooms (Sverdrup, 1953; Huisman *et al.*,
507 1999; Banse, 1994) are not relevant in the context of shallow and well-mixed coastal waters under the influence
508 of river plumes. In the studied region, the ecosystem does not evolve with mixed layer dynamics, as observed in
509 deeper environments. Both bays are permanently vertically mixed mainly by tides, and vertical stratification only
510 occurs on a thin surface layer due to river runoffs at short time scales. However, the IPGP is mainly driven and
511 limited by similar local environmental conditions in both bays. The ideal temperature (> 10 °C) and PAR (1300
512 $W m^{-2}$) for the IPGP are in agreement with those from previous studies conducted in similar coastal ecosystems
513 (*e.g.* Glé *et al.*, 2007; Townsend *et al.*, 1994; Trombetta *et al.*, 2019). Neap tidal conditions, weak wind (lower
514 than $3 m s^{-1}$) and weak river flow can also play a positive role to observe earlier IPGP according to the previous
515 studies (Ragueneau *et al.*, 1996; Tian *et al.*, 2011). The impact of wind direction on the IPGP is negligible.
516 Local changes in temperature, incident radiation, tidal conditions, wind conditions and river flow, induce
517 differences in detected IPGP. In this coastal temperate ecosystem, we observe that the beginning of the growing
518 period is limited by light (controlled by incident radiation, turbidity at this season), and water temperature. The
519 IPGP also occurs during low vertical mixing conditions.
520

521 The comparison of the individual importance of each environmental driver shows that temperature and
522 light penetration are the key environmental drivers in both bays. When light penetration is reduced by a combined
523 effect of PAR and turbidity (sediment resuspension), the delay of IPGP can be amplified, especially in the Bay of
524 Vilaine. The importance of light availability in the timing and intensity of the spring bloom is also highlighted in
525 the North Sea (Wiltshire *et al.*, 2015), in the German Bight (Tian *et al.*, 2009) and along the UK South Coast
526 (Iriarte and Purdie, 2004).
527

528 4.4 Interannual evolutions of the IPGP

529

530 The IPGP in these two bays shows a strong interannual variability with initiation dates varying from late
531 winter to spring, depending on the environmental conditions. A mean difference of 50 days between the earliest
532 and latest IPGP dates is observed. It is important to note that the phytoplankton population during the IPGP is
533 always dominated in both bays by the same centric diatoms, genera *Chaetoceros* and *Skeletonema*, whose

534 abundance varies from year to year depending on climatic conditions (REPHY, 2021). None of the nutrient is
535 limiting the growing of phytoplankton at the IPGP (Table 4).

536
537 The earliest IPGP are observed and related to favorable environmental conditions early in the year. For
538 example, the IPGP can occur before day 50, associated with exceptionally weak wind and river flow in addition
539 to a sufficient PAR and nearly-optimal temperature of around 10 °C (e.g. 2010 in the Bay of Brest and 2012 in the
540 Bay of Vilaine). But if the environmental conditions are not favorable (e.g. 2017 and 2019 in both bays), the IPGP
541 is delayed. This can be due to: 1- strong wind during several days (not a single wind burst) combined with a weak
542 PAR and enhanced sometimes by high turbidity events which further limits the light penetration. 2- low SST.

543
544 The IPGP appears to be more controlled by local environmental drivers than by regional environmental
545 drivers, the IPGP being earlier in one site than in the other during half of the studied years: for example, the 2012
546 IPGP is early in the Bay of Vilaine (day 53), but late in the Bay of Brest (day 80), related to strong wind activity
547 and low PAR on the last bay. The offshore regional dynamics will induce limited impacts on local hydrodynamical
548 features that will change IPGP.

549
550 Changes in the IPGP over the last two decades has highlighted its evolution through two trends: it occurs
551 earlier each year until 2010, when the trend is reversed. Changes in environmental conditions over the last 20 years
552 was then studied to seek a possible concordance with one of the environmental drivers, but no significant trend
553 was detected. Because of global warming, earlier phytoplankton blooms are expected (Friedland *et al.*, 2018) but
554 not later IPGP as observed in our study regions. However, the mechanisms that trigger blooms in coastal
555 ecosystems - especially eutrophic ones - are not similar to the processes that influence blooms in the open ocean.
556 No link between trends in IPGP and environmental drivers has not been identified in the southern California Bight
557 from 1983 to 2000 (Kim *et al.*, 2009). By investigating long-term (1975-2005) daily data, Wiltshire *et al.* (2008)
558 also observe later phytoplankton blooms in the German bight, but no link to global warming was detected. Henson
559 *et al.* (2018) model a bloom shift of 5 days per decade from 2006 to 2025, with later blooms. A possible explanation
560 of these later IPGP may involve a lower spring SST (Hunter-Cervera *et al.*, 2016).

561 562 4.5 Extreme events

563
564 We show that a cold spell is likely to delay the IPGP if it occurs at the end of winter (after 20th February)
565 or/and if the cold spell lasts long enough (> 15 days). The drop in temperature related to the cold spell prevents
566 the IPGP in both bays. This is in accordance with the study of Gomez and Souissi (2008) in the English Channel
567 where cold spells can delay the date of IPGP, as a result of an increase in water column mixing. Cold spells may
568 drive local patterns by influencing the phytoplankton communities (Gomez and Souissi, 2008; Schlegel *et al.*,
569 2021).

570
571 Flood events have an influence on the phytoplankton biomass when they occur in spring, due to the supply
572 of nutrients. When they occur in late winter, nutrients are already at their maximum. The impact of floods on IPGP
573 is then due to the increase of the water turbulence and to the limitation of light by increasing the turbidity. The
574 IPGP can be delay only if floods are at least 15 days long. This scheme was also observed by Saeck *et al.* (2013)
575 along a river-estuary-bay continuum and explained by a shortened water residence time and limited-light due to
576 flood-induced turbidity in the coastal zone.

577
578 No relationship is observed between wind events and IPGP in both bays because they are weakly
579 stratified, contrary to open seas (*i.e.* Black Sea, Mikaelyan *et al.*, 2017). In coastal stratified regions (e.g. under
580 the influence of river plumes), strong wind and tidal mixing can enhance the mixing and break down stratification,
581 which does not favor phytoplankton growth (Joordens *et al.*, 2021). During the IPGP, except during floods, both
582 regions are weakly stratified and are then less sensitive to combined wind/tidal short events.

583 584 **5 Conclusions**

585
586 This study provides a new understanding of the IPGP dynamics in coastal temperate areas by using both
587 high and low-frequency *in situ* data, in combination with simulations from a 1DV model. Strong similarities are
588 found in both bays. An important interannual variability of the IPGP is observed, with a trend towards a later IPGP
589 over the last decade (2010-2020). We quantify the importance of environmental conditions on the IPGP. When
590 we compare observed IPGP with favorable environmental conditions and following sensitivity experiments with
591 the 1DV model, water temperature and turbidity (limiting light penetration in the water column) appear as the

592 main drivers explaining interannual IPGP variability. The IPGP is a complex mechanism, usually triggered by
593 more than one environmental parameter. The analysis of the influence of extreme events reveals that cold spells
594 and floods have a strong impact by delaying the IPGP when episodes are long enough and occur after winter. No
595 effect of wind bursts is detected.

596 While this study shows comparable IPGP dynamics when based on 1DV model simulations or *in situ*
597 observations, we will next investigate the effect on phytoplankton dynamics of a fully realistic hydrodynamics
598 (including horizontal and vertical advections; mixing processes; remote sources of nutrients from rivers) 3D
599 model. We will focus on exploring the variability of phytoplankton communities during IPGP to assess whether
600 community change is occurring, as observed in other studies and for other ecosystems (Ianson *et al.*, 2001;
601 Edwards and Richardson, 2004; Chivers *et al.*, 2020). When interannual evolutions in the phytoplankton growth
602 are explored, the detection and the understanding of harmful algal bloom dynamics can also be addressed based
603 on similar approaches. Further studies will be dedicated to the simulation of the coastal ecosystem in the future
604 based on numerical simulation through climate scenarios. The investigation of other contrasting coastal
605 environments will allow us to better understand and anticipate the expected impact of global change on coastal
606 phytoplankton dynamics.

607 **Author contributions**

608 CP, GC, AD, RV, PR-M and EGo conceptualized the study. PR-M, EGr and MR collected data. MP and GC
609 developed the model configuration. CP, GC, AD and RV drafted the first versions of the paper. CP carried out all
610 the analyses and wrote the final version of the paper. All authors contributed to the discussions and revisions of
611 the study.

612 **Acknowledgements**

613 We would like to acknowledge COAST-HF (<http://www.coast-hf.fr>), SOMLIT ([http://sommelit.epoc.u-](http://sommelit.epoc.u-bordeaux1.fr)
614 [bordeaux1.fr](http://sommelit.epoc.u-bordeaux1.fr)) and REPHY (<https://doi.org/10.17882/47248>) national observing networks, for providing data flux
615 readily available. COAST-HF and SOMLIT are components of the National Research Infrastructure ILICO. We
616 would like to thank the Shom for tidal data and also Météo-France for wind and solar flux products. We also thank
617 Dr Claire Labry for fruitful discussions and Dr Sally Close for her proofreading. We thank the referees for their
618 helpful and constructive comments.

619 **Financial support**

620 This study is part of the State-Region Plan Contract ROEC supported in part by the European Regional
621 Development Funds and the COXTCLIM project funded by the Loire-Brittany Water Agency, the Brittany region
622 and Ifremer.

623 **References**

- 624 Aminot, A., and Kerouel, R.: Hydrologie des écosystèmes marins. Paramètres et analyses, Editions de l'Ifremer,
625 336 p., ISBN 2-84433-133-5, 2004.
- 626
- 627 Banse, K.: Grazing and zooplankton production as key controls of phytoplankton production in the open
628 ocean, *Oceanography*, 7(1), 13-20, <https://www.jstor.org/stable/43925524>, 1994.
- 629 Barbosa, A., Domingues, R., and Galvão., H.: Environmental forcing of phytoplankton in a Mediterranean estuary
630 (Guadiana estuary, south-western Iberia): A decadal study of anthropogenic and climatic influences, *Estuaries and*
631 *Coasts*, doi:10.1007/ s12237-009-9200-x, 2010.
- 632 Bedford, J., Ostle, C., Johns, D. G., Atkinson, A., Best, M., Bresnan, E., ... and McQuatters-Gollop, A.: Lifeform
633 indicators reveal large-scale shifts in plankton across the North-West European shelf, *Global Change Biology*,
634 26(6), 3482-3497, doi:10.1111/gcb.15066, 2020.
- 635 Behrenfeld, M. J.: Abandoning Sverdrup's critical depth hypothesis on phytoplankton blooms, *Ecology*, 91(4),
636 977-989, doi:10.1890/09-1207, 2010.

637
638 Behrenfeld, M. J., Doney, S. C., Lima, I., Boss, E. S., and Siegel, D. A.: Annual cycles of ecological disturbance
639 and recovery underlying the subarctic Atlantic spring plankton bloom, *Global biogeochemical cycles*, 27(2), 526-
640 540, doi:10.1002/gbc.20050, 2013.

641
642 Beucher, C., Treguer, P., Corvaisier, R., Hapette, A. M., and Elskens, M.: Production and dissolution of biosilica,
643 and changing microphytoplankton dominance in the Bay of Brest (France), *Marine Ecology Progress Series*, 267,
644 57-69, doi:10.3354/meps267057, 2004.

645
646 Boss, E., and Behrenfeld, M.: In situ evaluation of the initiation of the North Atlantic phytoplankton bloom,
647 *Geophysical Research Letters*, 37(18), doi:10.1029/2010GL044174, 2010.

648
649 Bouman, H., Platt, T., Sathyendranath, S., and Stuart, V.: Dependence of light-saturated photosynthesis on
650 temperature and community structure, *Deep Sea Research Part I: Oceanographic Research Papers*, 52(7), 1284-
651 1299, doi:10.1016/j.dsr.2005.01.008, 2005.

652
653 Brody, S. R., Lozier, M. S., and Dunne, J. P.: A comparison of methods to determine phytoplankton bloom
654 initiation, *Journal of Geophysical Research, Oceans*, 118(5), 2345-2357, doi:10.1002/jgrc.20167, 2013.

655
656 Caracciolo, M., Beaugrand, G., Hélaouët, P., Gevaert, F., Edwards, M., Lizon, F., ... and Goberville, E.: Annual
657 phytoplankton succession results from niche-environment interaction, *Journal of Plankton Research*, 43(1), 85-
658 102, doi:10.1093/plankt/fbaa060, 2021.

659
660 Chapelle, A., Lazure, P., and Ménesguen, A.: Modelling eutrophication events in a coastal ecosystem. Sensitivity
661 analysis, *Estuarine, Coastal and Shelf Science*, 39(6), 529-548, doi:10.1016/S0272-7714(06)80008-9, 1994.

662
663 Charria, G., Lazure, P., Le Cann, B., Serpette, A., Reverdin, G., Louazel, S., Batifoulier, F., Dumas, F., Pichon,
664 A. and Morel, Y. Surface layer circulation derived from Lagrangian drifters in the Bay of Biscay. *Journal of*
665 *Marine Systems*, 109, 60-76, doi:10.1016/j.jmarsys.2011.09.015, 2013.

666
667 Chiswell, S. Calil, P. and Boyd, P. Spring blooms and annual cycles of phytoplankton: a unified
668 perspective. *Journal of Plankton Research*, 37(3), 500-508, doi:10.1093/plankt/fbv021, 2015.

669
670 Chivers, W. J., Edwards, M., and Hays, G. C.: Phenological shuffling of major marine phytoplankton groups over
671 the last six decades, *Diversity and Distributions*, 26(5), 536-548, doi:10.1111/ddi.13028, 2020.

672
673 Cloern, J. E.: Phytoplankton bloom dynamics in coastal ecosystems: a review with some general lessons from
674 sustained investigation of San Francisco Bay, California, *Reviews of Geophysics*, 34(2), 127-168,
675 doi:10.1029/96RG00986, 1996.

676
677 Cocquempot, L., Delacourt, C., Paillet, J., Riou, P., Aucan, J., Castelle, B., Charria, G., Claudet, J., Conan, P.,
678 Coppola, L., Hocdé, R., Planes, S., Raimbault, P., Savoye, N., Testut, L., and Vuillemin, R.: Coastal Ocean and
679 Nearshore Observation: A French Case Study, *Frontiers in Marine Science*, 6(324), 1-17,
680 doi:10.3389/fmars.2019.00324, 2019.

681
682 Cook, P. L., Holland, D. P., and Longmore, A. R.: Effect of a flood event on the dynamics of phytoplankton and
683 biogeochemistry in a large temperate Australian lagoon, *Limnology and Oceanography*, 55(3), 1123-1133,
684 doi:10.4319/lo.2010.55.3.1123, 2010.

685
686 Cugier, P., Billen, G., Guillaud, J. F., Garnier, J., and Ménesguen, A.: Modelling the eutrophication of the Seine
687 Bight (France) under historical, present and future riverine nutrient loading, *Journal of Hydrology*, 304(1-4), 381-
688 396, doi:10.1016/j.jhydrol.2004.07.049, 2005.

689
690 Del Amo, Y., Le Pape, O., Tréguer, P., Quéguiner, B., Ménesguen, A., and Aminot, A.: Impacts of high-nitrate
691 freshwater inputs on macrotidal ecosystems. I. Seasonal evolution of nutrient limitation for the diatom-dominated
692 phytoplankton of the Bay of Brest (France), *Marine Ecology Progress Series*, 161, 213-224, doi:10.5194/bg-16-
693 1361-2019, 1997.

694

695 Edwards, M., and Richardson, A. J.: Impact of climate change on marine pelagic phenology and trophic
696 mismatch, *Nature*, 430(7002), 881-884, doi:10.1038/nature02808, 2004.
697

698 Farcy, P., Durand, D., Charria, G., Painting, S.J., Tamminem, T., Collingridge, K., Grémare, A.J., Delauney, L.,
699 and Puillat, I.: Toward a European coastal observing network to provide better answers to science and to societal
700 challenges; the JERICO research infrastructure, *Frontiers in Marine Science*, 6, 1–13,
701 doi:10.3389/fmars.2019.00529, 2019.
702

703 Ferrer, L., Fontán, A., Mader, J., Chust, G., González, M., Valencia, V., Uriarte, Ad. and Collins, M.B. Low-
704 salinity plumes in the oceanic region of the Basque Country. *Continental Shelf Research* 29 (8), 970–984,
705 doi:10.1016/j.csr.2008.12.014, 2009.
706

707 Frère, L., Paul-Pont, I., Rinnert, E., Petton, S., Jaffré, J., Bihannic, I., Soudant, P., Lambert, C. and Huvet, A.:
708 Influence of environmental and anthropogenic factors on the composition, concentration and spatial distribution
709 of microplastics : a case study of the Bay of Brest (Brittany, France), *Environ. Pollut*, 225, 211–222,
710 doi:10.1016/j.envpol.2017.03.023, 2017.
711

712 Friedland, K. D., Mouw, C. B., Asch, R. G., Ferreira, A. S. A., Henson, S., Hyde, K. J., ... and Brady, D. C.:
713 Phenology and time series trends of the dominant seasonal phytoplankton bloom across global scales, *Global
714 Ecology and Biogeography*, 27(5), 551-569, doi:10.1111/geb.12717, 2018.
715

716 Glé, C., Del Amo, Y., Bec, B., Sautour, B., Froidefond, J. M., Gohin, F., Maurer, D., Plus, M., Laborde, P., and
717 Chardy, P.: Typology of environmental conditions at the onset of winter phytoplankton blooms in a shallow
718 macrotidal coastal ecosystem, Arcachon Bay (France), *Journal of plankton research*, 29(11), 999-1014,
719 doi:10.1093/plankt/fbm074, 2007.
720

721 Gohin, F., Van der Zande, D., Tilstone, G., Eleveld, M. A., Lefebvre, A., Andrieux-Loyer, F., Blauw, A. N.,
722 Bryère, P., Devreker, D., Garnesson, P., Hernández Fariñas, T., Lamaury, Y., Lampert, L., Lavigne, H., Menet-
723 Nedelec, F., Pardo, S., and Saulquin, B.: Twenty years of satellite and in situ observations of surface chlorophyll-
724 a from the northern Bay of Biscay to the eastern English Channel. Is the water quality improving ? *Remote Sensing
725 of Environment*, 233(September), 111343, doi:10.1016/j.rse.2019.111343, 2019.
726

727 Gomez, F., and Souissi, S.: The impact of the 2003 heat wave and the 2005 cold wave on the phytoplankton in the
728 north-eastern English Channel, *Comptes Rendues Biologies*, 331(9), 678-685, doi:10.1016/j.crvi.2008.06.005,
729 2008.

730 Grasso F., Le Hir P., and Bassoullet P.: Numerical modelling of mixed-sediment consolidation, *Ocean Dynamics*,
731 65(4), 607– 616, doi:10.1007/s10236-015-0818-x, 2015.

732 Hartigan, J., and Wong, M.: Algorithm AS 136: A K-Means Clustering Algorithm. *Journal of the Royal Statistical
733 Society, Series C (Applied Statistics)*, 28:1, 100-108, doi:2346830, 1979.
734

735 Henson, S. A., Cole, H. S., Hopkins, J., Martin, A. P., and Yool, A.: Detection of climate change-driven trends in
736 phytoplankton phenology, *Global Change Biology*, 24(1), e101-e111, doi:10.1111/gcb.13886, 2018.
737

738 Huisman, J. E. F., van Oostveen, P., and Weissing, F. J.: Critical depth and critical turbulence: two different
739 mechanisms for the development of phytoplankton blooms, *Limnology and oceanography*, 44(7), 1781-1787,
740 doi.org/10.4319/lo.1999.44.7.1781, 1999.
741

742 Hunter-Cevera, K. R., Neubert, M. G., Olson, R. J., Solow, A. R., Shalapyonok, A., and Sosik, H. M.:
743 Physiological and ecological drivers of early spring blooms of a coastal phytoplankter, *Science*, 354(6310), 326-
744 329, doi:10.1126/science.aaf8536, 2016.
745

746 Husson, B., Hernández-Fariñas, T., Le Gendre, R., Schapira, M., and Chapelle, A.: Two decades of Pseudo-
747 nitzschia spp. blooms and king scallop (*Pecten maximus*) contamination by domoic acid along the French Atlantic
748 and English Channel coasts: Seasonal dynamics, spatial heterogeneity and interannual variability, *Harmful
749 Algae*, 51, 26-39, doi:10.1016/j.hal.2015.10.017, 2016.
750

751 Ianson, D., Pond, S., and Parsons, T.: The spring phytoplankton bloom in the coastal temperate ocean: growth
752 criteria and seeding from shallow embayments, *Journal of oceanography*, 57(6), 723-734,
753 doi.org/10.1023/A:1021288510407, 2001.

754
755 IPCC: Summary for Policymakers. In: *Climate Change 2021: The Physical Science Basis. Contribution of*
756 *Working Group I to the Sixth Assessment Report of the Intergovernmental Panel on Climate Change* [Masson-
757 Delmotte, V., P. Zhai, A. Pirani, S. L. Connors, C. Péan, S. Berger, N. Caud, Y. Chen, L. Goldfarb, M. I. Gomis,
758 M. Huang, K. Leitzell, E. Lonnoy, J.B.R. Matthews, T. K. Maycock, T. Waterfield, O. Yelekçi, R. Yu and B. Zhou
759 (eds.)], Cambridge University Press, In Press, 2021.

760
761 Iriarte, A., and Purdie, D. A.: Factors controlling the timing of major spring bloom events in an UK south coast
762 estuary, *Estuarine, Coastal and Shelf Science*, 61(4), 679-690, doi:10.1016/j.ecss.2004.08.002, 2004.

763
764 Isemer, H.-J. and Hasse, L. The Bunker Climate Atlas of the North Atlantic Ocean, 2 Vols. Springer, Berlin. 218-
765 252, 1985.

766
767 Joordens, J. C. A., Souza, A. J., & Visser, A.: The influence of tidal straining and wind on suspended matter and
768 phytoplankton distribution in the Rhine outflow region. *Continental Shelf Research*, 21(3), 301-325,
769 doi:10.1016/S0278-4343(00)00095-9, 2001.

770
771 Kromkamp, J. C., and Van Engeland, T.: Changes in phytoplankton biomass in the western Scheldt estuary during
772 the period 1978-2006, *Estuaries and Coasts*, 33(2), 270–285, doi:10.1007/s12237-009-9215-3, 2010.

773
774 Kim, H. J., Miller, A. J., McGowan, J., and Carter, M. L.: Coastal phytoplankton blooms in the Southern California
775 Bight, *Progress in Oceanography*, 52(2), 137-147, doi:10.1016/j.pocean.2009.05.002, 2009.

776
777 Lazure, P., Jégou, A.-M. and Kerdreux, M. Analysis of salinity measurements near islands on the French
778 continental shelf of the Bay of Biscay. *Scientia Marina* 70 (S1), 7–14, 2006.

779
780 Lazure, P., and Dumas, F.: An external–internal mode coupling for a 3D hydrodynamical model for applications
781 at regional scale (MARS), *Advances in water resources*, 31(2), 233-250, doi:10.1016/j.advwatres.2007.06.010,
782 2008.

783
784 Lazure, P., and Jégou, A. M.: 3D modelling of seasonal evolution of Loire and Gironde plumes on Biscay Bay
785 continental shelf, *Oceanologica acta*, 21(2), 165-177, doi:10.1016/S0399-1784(98)80006-6, 1998.

786
787 Le Boyer, A., Charria, G., Le Cann, B., Lazure, P., and Marié, L. Circulation on the shelf and the upper slope of
788 the Bay of Biscay. *Continental Shelf Research*, 55, 97-107, doi:10.1016/j.csr.2013.01.006, 2013.

789
790 Lefort, T., and Gasol, J. M.: Short-time scale coupling of picoplankton community structure and single-cell
791 heterotrophic activity in winter in coastal NW Mediterranean Sea waters, *Journal of plankton research*, 36(1),
243-258, doi:10.1093/plankt/ftb073, 2014.

792
793 Le Hir P., Cayocca F., and Waeles B.: Dynamics of sand and mud mixtures: A multiprocess-based modelling
strategy, *Continental Shelf Research*, 31(10), S135– S149, doi:10.1016/j.csr.2010.12.009, 2011.

794
795 Lehmuskero, A., Skogen Chauton, M., and Boström, T.: Light and photosynthetic microalgae: A review of
796 cellular- and molecular-scale optical processes, *Progress in Oceanography*, 168(September), 43–56,
doi:10.1016/j.pocean.2018.09.002, 2018.

797
798 Le Pape, O., and Menesguen, A.: Hydrodynamic prevention of eutrophication in the Bay of Brest (France), a
799 modelling approach, *Journal of Marine Systems*, 12(1-4), 171-186, doi:10.1016/S0924-7963(96)00096-6, 1997.

800
801 Liu, X., Dunne, J. P., Stock, C. A., Harrison, M. J., Adcroft, A., and Resplandy, L.: Simulating water residence
802 time in the coastal ocean: A global perspective, *Geophysical Research Letters*, 46(23), 13910-13919, doi:
803 10.1029/2019GL085097, 2019.

804 Ménesguen, A., Dussauze, M., and Dumas, F.: Designing optimal scenarios of nutrient loading reduction in a
805 WFD/MSFD perspective by using passive tracers in a biogeochemical-3D model of the English Channel/Bay of
806 Biscay area, *Ocean & Coastal Management*, 163, 37-53, doi:10.1016/j.ocecoaman.2018.06.005, 2018.
807

808 Ménesguen, A., Dussauze, M., Dumas, F., Thouvenin, B., Garnier, V., Lecornu, F., and Répécaud, M.: Ecological
809 model of the Bay of Biscay and English Channel shelf for environmental status assessment part 1: Nutrients,
810 phytoplankton and oxygen, *Ocean Modelling*, 133, 56-78, doi.org/10.1016/j.ocemod.2018.11.002, 2019.

811 Mengual B., Le Hir P., Cayocca F., and Garlan T.: Modelling fine sediment dynamics: Towards a common erosion
812 law for fine sand, mud and mixtures, *Water*, 9, 564, doi:10.3390/w9080564, 2017.

813 Mikaelyan, A., Chasovnikov, V., Kubryakov, A., and Stanichny, S.: Phenology and drivers of the winter-spring
814 phytoplankton bloom in the open Black Sea: The application of Sverdrup's hypothesis and its refinements,
815 *Progress in Oceanography*, 151, 163-176, doi:10.1016/j.pocean.2016.12.006, 2017.

816 Moncheva, S., Gotsis-Skretas, O., Pagoub, K., and Krasteva, A.: Phytoplankton Blooms in Black Sea and
817 Mediterranean Coastal Ecosystems Subjected to Anthropogenic Eutrophication: Similarities and
818 Differences, *Estuarine, Coastal and Shelf Science*, 53, 281-295, doi:10.1006/ecss.2001.0767, 2001.
819

820 Oliver, E., Donat, M., Burrows, M., Moore, P., Smale, D., Alexandra, L., Benthuisen, J., Feng, M., Sen Gupta, A.,
821 Hobday, A., Holbrook, N., Perkins-Kirkpatrick, S., Scannell, H., Straub, S. and Wernberg, T.: Longer and more
822 frequent marine heatwaves over the past century, *Nature communications*, 9 :1324, doi:10.1038/s41467-018-
823 03732-9, 2018.
824

825 Paerl, H. W., Hall, N. S., Peierls, B. L., and Rossignol, K. L.: Evolving paradigms and challenges in estuarine and
826 coastal eutrophication dynamics in a culturally and climatically stressed world, *Estuaries and coasts*, 37(2), 243-
827 258, doi.org/10.1007/s12237-014-9773-x, 2014.
828

829 Peierls, B. L., Hall, N. S., and Paerl, H. W.: Non-monotonic responses of phytoplankton biomass accumulation to
830 hydrologic variability: a comparison of two coastal plain North Carolina estuaries, *Estuaries and coasts*, 35(6),
831 1376-1392, doi.org/10.1007/s12237-012-9547-2, 2012.
832

833 Petton, S., Pouvreau, S., and Dumas, F. Intensive use of Lagrangian trajectories to quantify coastal area dispersion,
834 *Ocean Dynamics*, 70(4), 541-559, doi.org/10.1007/s10236-019-01343-6, 2020.
835

836 Philippart, C. J. M., van Iperen, J. M., Cadée, G. C., and Zuur, A. F.: Long-term field observations on seasonality
837 in chlorophyll-a concentrations in a shallow coastal marine ecosystem, the Wadden Sea, *Estuaries and Coasts*,
838 33(2), 286–294, doi:10.1007/s12237-009-9236-y, 2010.
839

840 Pingree, R.D. and Le Cann, B. Celtic and Armorican slope and shelf residual currents. *Progress in Oceanography*
841 23 (4), 303–338, doi:10.1016/0079-6611(89)90003-7, 1989.
842

843 Plus, M., Thouvenin, B., Andrieux, F., Dufois, F., Ratmaya, W., Souchu, P. Diagnostic étendu de l'eutrophisation
844 (DIETE). Modélisation biogéochimique de la zone Vilaine-Loire avec prise en compte des processus
845 sédimentaires. Description du modèle Bloom (Biogeochemical Coastal Ocean Model). RST/LER/MPL/21.15.
846 <https://archimer.ifremer.fr/doc/00754/86567/>, 2021.
847

848 Poppeschi, C., Charria, G., Goberville, E., Rimmelin-Maury, P., Barrier, N., Petton, S., Unterberger, M.,
849 Grossteffan, E., Repeccaud, M., Quémener, L., Le Roux, J.-F., and Tréguer, P.: Unraveling salinity extreme events
850 in coastal environments: a winter focus on the bay of Brest, *Frontiers in Marine Science*, 8,
851 705403, doi:10.3389/fmars.2021.705403, 2021.
852

853 Quéguiner, B., and Tréguer, P.: Studies on the Phytoplankton in the Bay of Brest (Western Europe), Seasonal
854 Variations in Composition, Biomass and Production in Relation to Hydrological and Chemical Features (1981—
855 1982), *Botanica Marina*, 27, 449-459, 1984.
856

857 Ragueneau, O., Quéguiner, B. and Tréguer, P.: Contrast in biological responses to tidally-induced vertical mixing
858 for two macrotidal ecosystems of western Europe, *Estuarine, Coastal and Shelf Science*, 42, 645-665,
859 doi:10.1006/ecss.1996.0042, 1996.
860

861 Ragueneau, O., Chauvaud, L., Leynaert, A., Thouzeau, G., Paulet, Y. M., Bonnet, S., Lorrain, A., Grall, J.,
862 Corvaisier, R., Le Hir, M., Jean, F., and Clavier, J.: Direct evidence of a biologically active coastal silicate pump:
863 ecological implications, *Limnology and Oceanography*, 47(6), 1849-1854, doi.org/10.4319/lo.2002.47.6.1849,
864 2002.

865
866 Ragueneau, O., Raimonet, M., Mazé, C., Coston-Guarini, J., Chauvaud, L., Danto, A., Grall, J., Jean, F., Paulet
867 Y.-M., and Thouzeau, G.: The impossible sustainability of the Bay of Brest ? Fifty years of ecosystem changes,
868 interdisciplinary knowledge construction and key questions at the science-policy-community interface, *Frontiers*
869 *in Marine Science*, 5, 124, doi.org/10.3389/fmars.2018.00124, 2018.

870
871 Ratmaya, W., Soudant, D., Dalmon-Monviola, J., Plus, M., Cochennec-Laureau, N., Goubert, E., Andrieux-Loyer,
872 F., Barillé, L. and Souchu, P.: Reduced phosphorus loads from the Loire and Vilaine rivers were accompanied by
873 increasing eutrophication in the Vilaine Bay (south Brittany, France), *Biogeosciences*, 16:1361-1380,
874 doi:10.5194/bg-16-1361-2019, 2019.

875
876 Ratmaya, W., Laverman, AM., Rabouille, C., Akbarzadeh, Z., Andrieux-Loyer, F., Barillé, L., Barillé, A-L., Le
877 Merrer, Y., and Souchu, P.: Temporal and spatial variations in benthic nitrogen cycling in a temperate macro-tidal
878 coastal ecosystem : Observation and modeling, *Continental Shelf Research*, doi:10.1016/j.csr.2022.104649, 2022.

879
880 Répécaud, M., Quemener, L., Charria, G., Pairaud, I., Rimmelin, P., Claquin, P., Jacqueline, F., Lefebvre, A.,
881 Facq, J.V., Retho, M., and Verney, R.: National observation infrastructure: an example of a fixed-platforms
882 network along the French Coast: COAST HF, OCEANS IEE, pp. 1-6, doi:10.1109/OCEANSE.2019.8867451,
883 2019.

884
885 REPHY: French Observation and Monitoring program for Phytoplankton and Hydrology in coastal waters,
886 REPHY dataset - French Observation and Monitoring program for Phytoplankton and Hydrology in coastal waters.
887 Metropolitan data, SEANOE, doi:10.17882/47248, 2021.

888
889 Retho, M., Quemener, L., Le Gall, C., Repecaud, M., Souchu, P., Gabellec, R. and Manach, S.: MOLIT Vilaine
890 data and metadata from Coriolis Data Centre, SEANOE, doi:10.17882/46529, 2020.

891
892 Rimmelin-Maury, P., Charria, G., Repecaud, M., Quemener, L., Beaumont, L. Guillot, A., Gautier, L., Prigent, S.,
893 Le Becque, T., Bihannic, I., Bonnat, A., Le Roux, J-F., Grossteffan, E., Devesa, J., and Bozec, Y.: Iroise buoys
894 data from Coriolis data center as core parameter support for Brest Bay and Iroise sea studies, SEANOE, 2020.

895
896 Rossignol-Strick, M.: A marine anoxic event on the Brittany coast, July 1982, *Journal of Coastal Research*, 11-
897 20, <https://www.jstor.org/stable/4297005>, 1985.

898
899 Rumyantseva, A., Henson, S., Martin, A., Thompson, A. F., Damerell, G. M., Kaiser, J., and Heywood, K. J.:
900 Phytoplankton spring bloom initiation: The impact of atmospheric forcing and light in the temperate North
901 Atlantic, *Ocean. Progress in oceanography*, 178, 102202, doi:10.1016/j.pocean.2019.102202, 2019.

902
903 Saeck, E. A., Hadwen, W. L., Rissik, D., O'Brien, K. R., and Burford, M. A.: Flow events drive patterns of
904 phytoplankton distribution along a river–estuary–bay continuum, *Marine and Freshwater Research*, 64(7), 655-
905 670, doi:10.1071/MF12227, 2013.

906
907 Sathyendranath, S., Ji, R., and Browman, H. I.: Revisiting Sverdrup's critical depth hypothesis, *ICES Journal of*
908 *Marine Science*, 72(6), 1892-1896, doi:10.1093/icesjms/fsv110, 2015.

909
910 Schlegel, R. W., Darmaraki, S., Benthuyssen, J. A., Filbee-Dexter, K., and Oliver, E. C.: Marine cold-
911 spells, *Progress in Oceanography*, 198, 102684, doi.org/10.1101/2021.10.18.464880, 2021.

912
913 Serre-Fredj, L., Jacqueline, F., Navon, M., Izabel, G., Chasselín, L., Jolly, O., ... and Claquin, P.: Coupling high
914 frequency monitoring and bioassay experiments to investigate a harmful algal bloom in the Bay of Seine (French-
915 English Channel), *Marine Pollution Bulletin*, 168, 112387, doi:10.1016/j.marpolbul.2021.112387, 2021.

916
917 Smetacek, V., & Cloern, J. E.: On phytoplankton trends, *Science*, 319(5868), 1346-1348, doi:
918 10.1126/science.1151330, 2008.

919

920 Sommer, U., Adrian, R., De Senerpont Domis, L., Elser, J. J., Gaedke, U., Ibelings, B., Jeppesen, E., Lürling, M.,
921 Molinero, J. C., Mooij, W. M., van Donk, E., and Winder, M.: Beyond the Plankton Ecology Group (PEG) model:
922 mechanisms driving plankton succession, *Annual review of ecology, evolution, and systematics*, 43, 429-448,
923 doi:10.1146/annurev-ecolsys-110411-160251, 2012.

924

925 Stockwell, J. D., Doubek, J. P., Adrian, R., Anneville, O., Carey, C. C., Carvalho, L., ... and Wilson, H. L.: Storm
926 impacts on phytoplankton community dynamics in lakes, *Global change biology*, 26(5), 2756-2784,
927 doi:10.1111/gcb.15033, 2020.

928

929 Sverdrup, H.: On vernal blooming of phytoplankton, *Conseil Exp. Mer*, 18, 287-295, 1953.

930

931 Thyssen, M., Tarran, G. A., Zubkov, M. V., Holland, R. J., Grégori, G., Burkill, P. H., and Denis, M.: The
932 emergence of automated high-frequency flow cytometry: revealing temporal and spatial phytoplankton variability,
933 *Journal of plankton research*, 30(3), 333-343, doi:10.1093/plankt/fbn005, 2008.

934

935 Tian, T., Merico, A., Su, J., Staneva, J., Wiltshire, K., and Wirtz, K.: Importance of resuspended sediment
936 dynamics for the phytoplankton spring bloom in a coastal marine ecosystem, *Journal of Sea Research*, 62(4), 214-
937 228, doi:10.1016/j.seares.2009.04.001, 2009.

938

939 Tian, T., Su, J., Flöser, G., Wiltshire, K., and Wirtz, K.: Factors controlling the onset of spring blooms in the
940 German Bight 2002–2005: light, wind and stratification, *Continental Shelf Research*, 31(10), 1140-1148,
941 doi:10.1016/j.csr.2011.04.008, 2011.

942

943 Townsend, D. W., Cammen, L. M., Holligan, P. M., Campbell, D. E., and Pettigrew, N. R.: Causes and
944 consequences of variability in the timing of spring phytoplankton blooms, *Deep Sea Research Part I:
945 Oceanographic Research Papers*, 41(5-6), 747-765, doi:10.1016/0967-0637(94)90075-2, 1994.

946

947 Trombetta, T., Vidussi, F., Mas, S., Parin, D., Simier, M., and Mostajir, B.: Water temperature drives
948 phytoplankton blooms in coastal waters, *PloS one*, 14(4), e0214933, doi:10.1371/journal.pone.0214933, 2019.

949

950 Wiltshire, K. H., Malzahn, A. M., Wirtz, K., Greve, W., Janisch, S., Mangelsdorf, P., ... and Boersma, M.:
951 Resilience of North Sea phytoplankton spring bloom dynamics: An analysis of long-term data at Helgoland
952 Roads, *Limnology and Oceanography*, 53(4), 1294-1302, doi:10.4319/lo.2008.53.4.1294, 2008.

953

954 Wiltshire, K. H., Boersma, M., Carstens, K., Kraberg, A. C., Peters, S., and Scharfe, M.: Control of phytoplankton
955 in a shelf sea: determination of the main drivers based on the Helgoland Roads Time Series, *Journal of Sea
956 Research*, 105, 42-52, doi:10.1016/j.seares.2015.06.022, 2015.

957

958

959

960

961

962

963

964

965

966

967

968

969

970

971

972

973

974

975

976

977

978

979

980

981
 982
 983
 984
 985
 986
 987
 988
 989
 990
 991
 992
 993
 994
 995
 996
 997
 998
 999
 1000
 1001
 1002
 1003
 1004
 1005
 1006
 1007
 1008
 1009
 1010
 1011
 1012
 1013
 1014
 1015
 1016
 1017
 1018
 1019
 1020
 1021
 1022
 1023
 1024
 1025
 1026
 1027
 1028

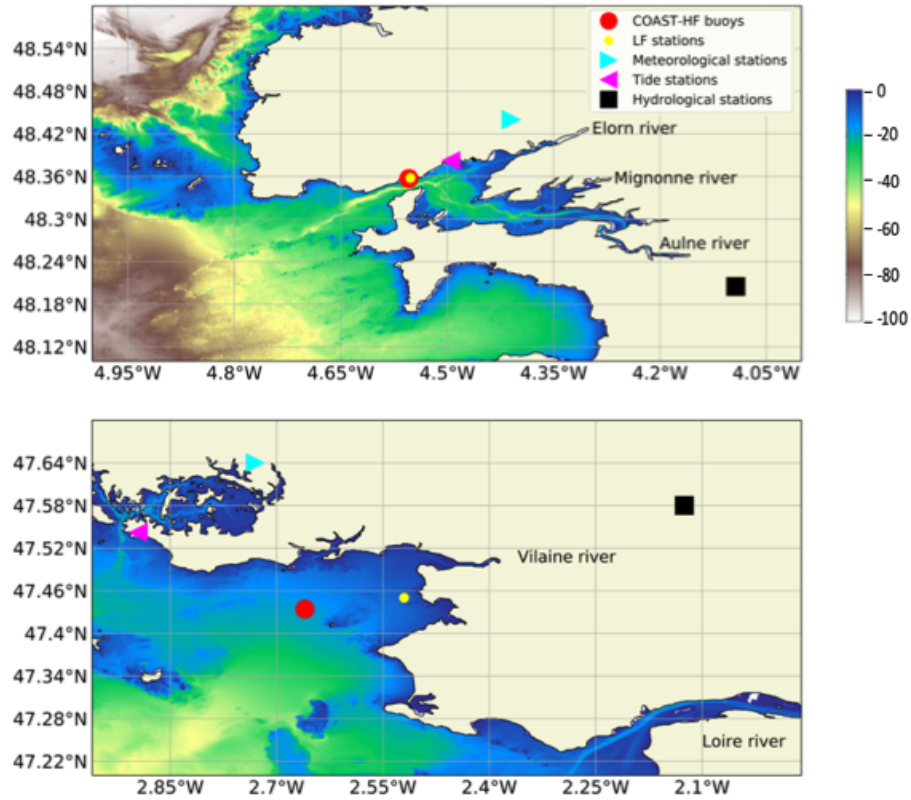


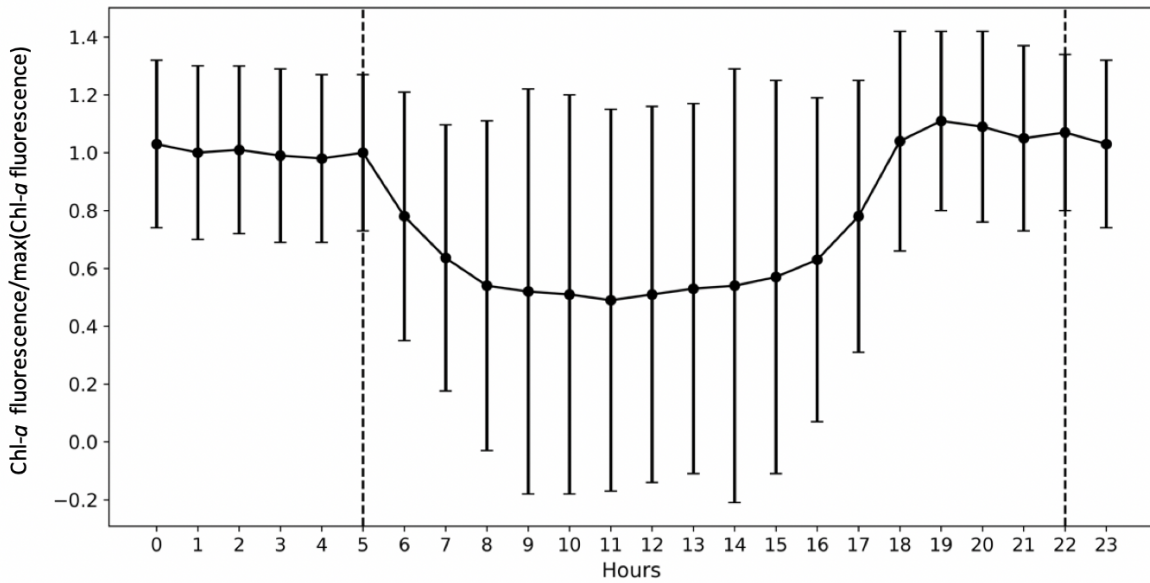
Figure 1: Location of the sampling sites: COAST-HF-Iroise and COAST-HF-Molit buoys (red circles); SOMLIT-Brest and REPHY-Loscolo sampling stations (yellow circles); Brest and Crouesty tide gauge stations (blue triangles); Guipavas and Vannes-Séné meteorological stations (purple triangles); hydrological stations of the Aulne and Vilaine rivers (black squares) with the Loire station off the map.

Parameters	Bay of Brest	Bay of Vilaine
Dissolved O ₂ ($mg L^{-1}$)	9	10
Mesozooplankton ($\mu mol N L^{-1}$)	0.05	0.1
Microzooplankton ($\mu mol N L^{-1}$)	0.05	0.05
Dinoflagellates ($\mu mol N L^{-1}$)	0.05	0.1
Diatoms ($\mu mol N L^{-1}$)	0.5	0.5
Soluble reactive phosphorus ($\mu mol L^{-1}$)	0.5	0.8
Silicic acid ($\mu mol L^{-1}$)	10	30

Nitrate ($\mu\text{mol L}^{-1}$)	16	30
Ammonium ($\mu\text{mol L}^{-1}$)	0.5	0.25
Coarse sand (g L^{-1})	0	0
Fine sand (g L^{-1})	0	0
Mud (g L^{-1})	0.03	0.05

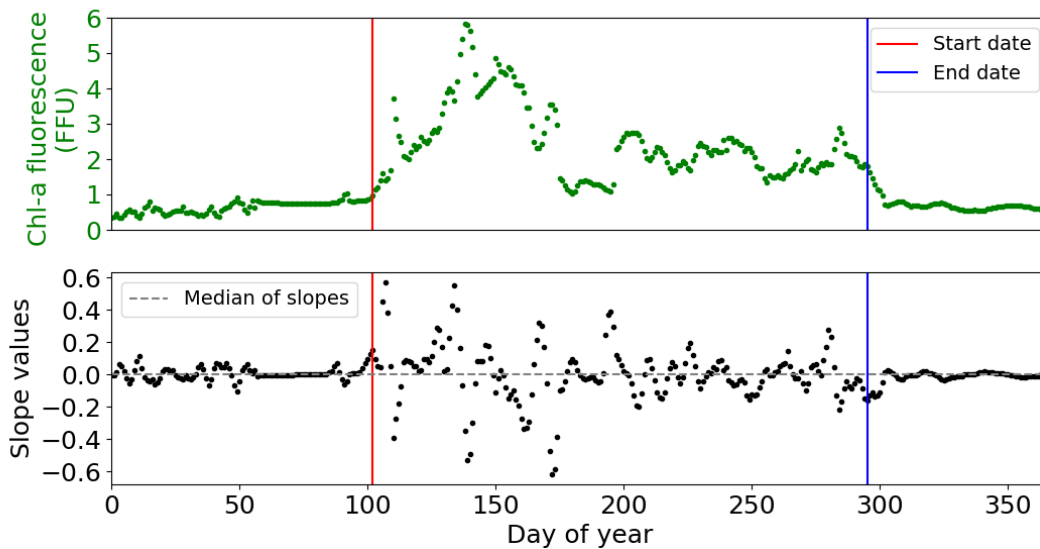
1029
1030
1031
1032

Table 1: Initial conditions in the water column for the MARS-1DV model for the beginning of the simulation on the February 15th.



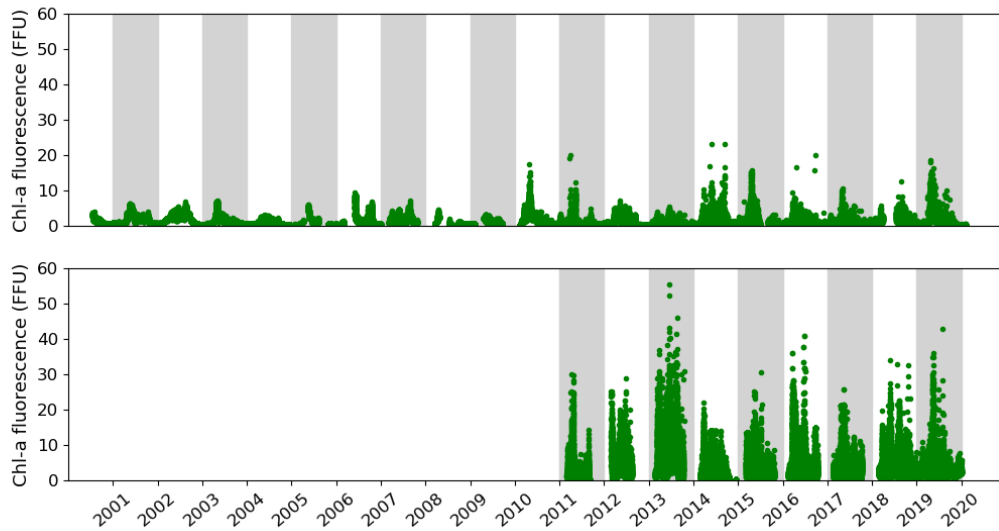
1033
1034
1035
1036
1037

Figure 2: Importance of the Quenching effect on Chl-*a* fluorescence is represented by COAST-HF-Iroise data from 2000 to 2019. The standard deviation is represented by vertical black bars. The dashed lines represent the beginning and end of the selected values for the rest of the study from 10 pm to 5 am.



1038
1039
1040
1041

Figure 3: Example of detection of the start (red line) and end (blue line) of the phytoplankton growing period in 2001 at COAST-HF-Iroise. The threshold value - median of slopes - is represented by a dotted grey line.



1042
1043
1044
1045
1046
1047

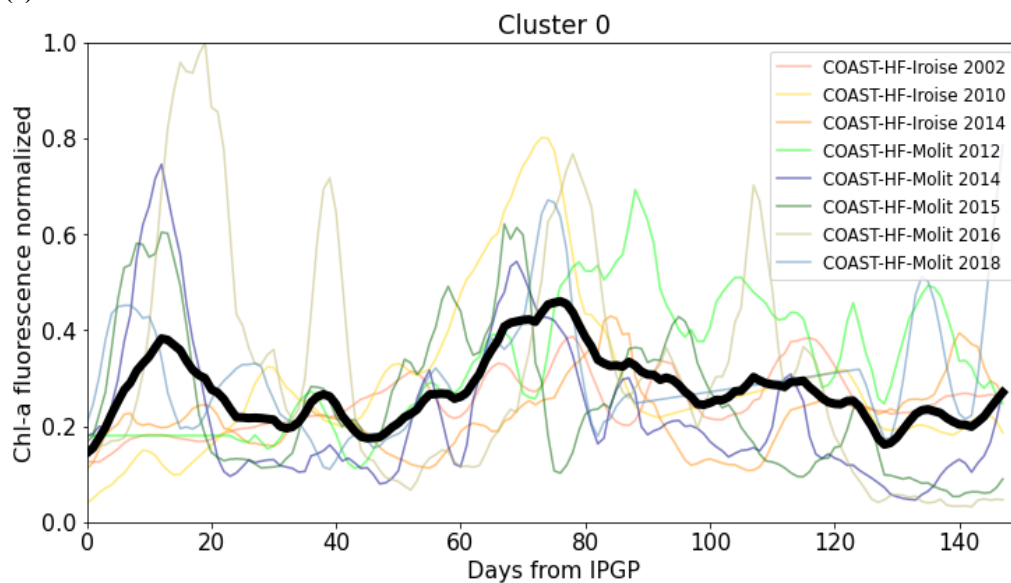
Figure 4: Temporal changes in the *in situ* Chl-*a* fluorescence measured in the Bay of Brest (top) and the Bay of Vilaine (bottom).

	Start date (Day of year)	End date (Day of year)	Duration (Days)	Cumulative Chl- <i>a</i> fluorescence (FFU)
	<i>Min - Median - Max</i>	<i>Min - Median - Max</i>	<i>Min - Median - Max</i>	<i>Min - Median - Max</i>
Bay of Brest (2001-2019)	50 - 69 - 102	253 - 274 - 308	165 - 200 - 256	217 - 364 - 567
Bay of Vilaine (2011-2019)	53 - 68 - 93	218 - 269 - 316	165 - 179 - 239	276 - 582 - 1406

1048
1049
1050
1051
1052
1053
1054

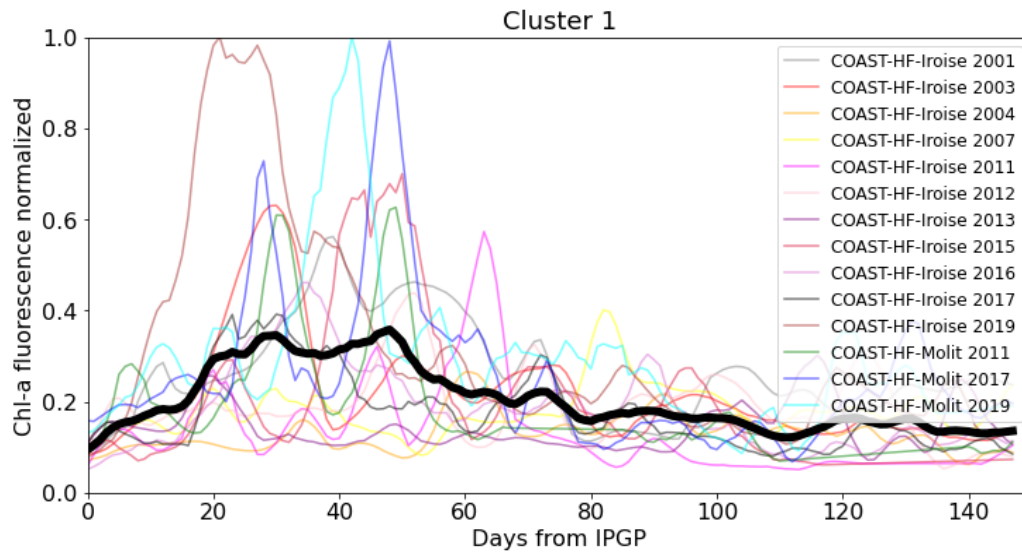
Table 2: Global characteristics of the phytoplankton growing period in the Bay of Brest and in the Bay of Vilaine.

(a)



1055
1056
1057

1058 (b)
1059



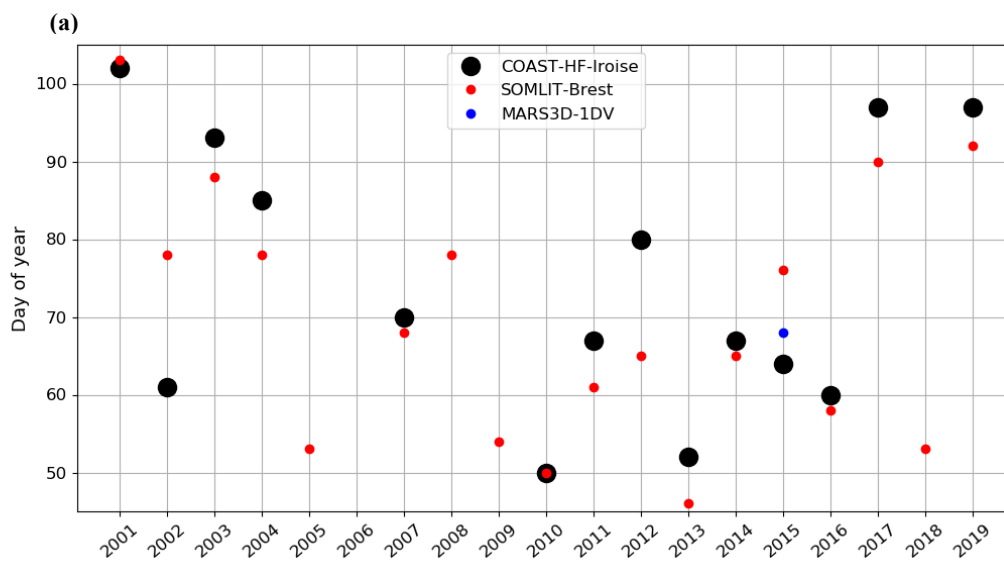
1060
1061
1062
1063
1064
1065
1066

Figure 5: (a) Cluster 0 and (b) cluster 1 representative of the patterns of the phytoplankton growing period observed in both bays. The median pattern is drawn in bold.

Year	2001	2002	2003	2004	2005	2006	2007	2008	2009	2010	2011	2012	2013	2014	2015	2016	2017	2018	2019
Bay of Brest COAST-HF-Iroise	1	0	1	1			1			0	1	1	1	0	1	1	1		1
Bay of Vilaine COAST-HF-Molit											1	0	X	0	0	0	1	0	1

1067
1068
1069
1070
1071
1072
1073

Table 3: Cluster group assigned to each annual phytoplankton growing period on both sites. Grey boxes represent years with missing data. The cross represents the year 2013 of the Bay of Vilaine not considered.



1074
1075
1076
1077

(b)

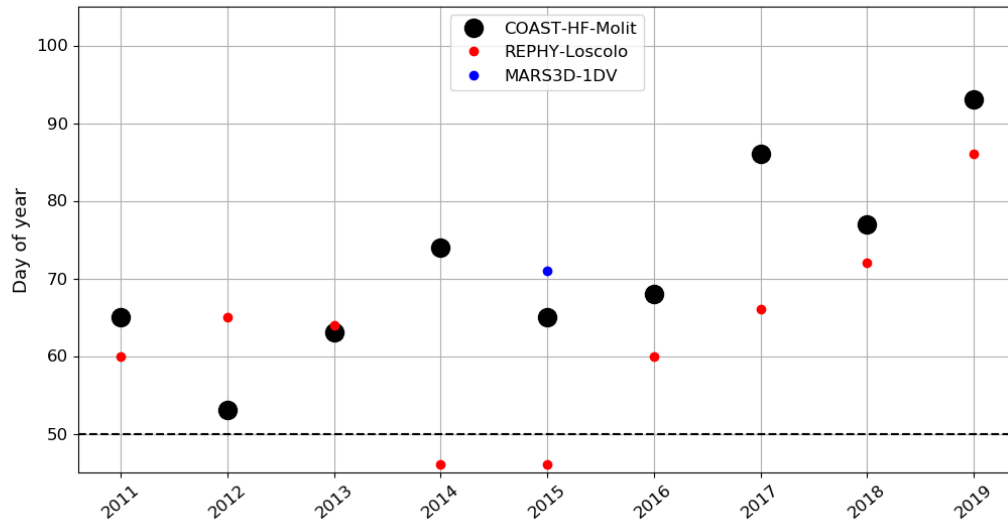
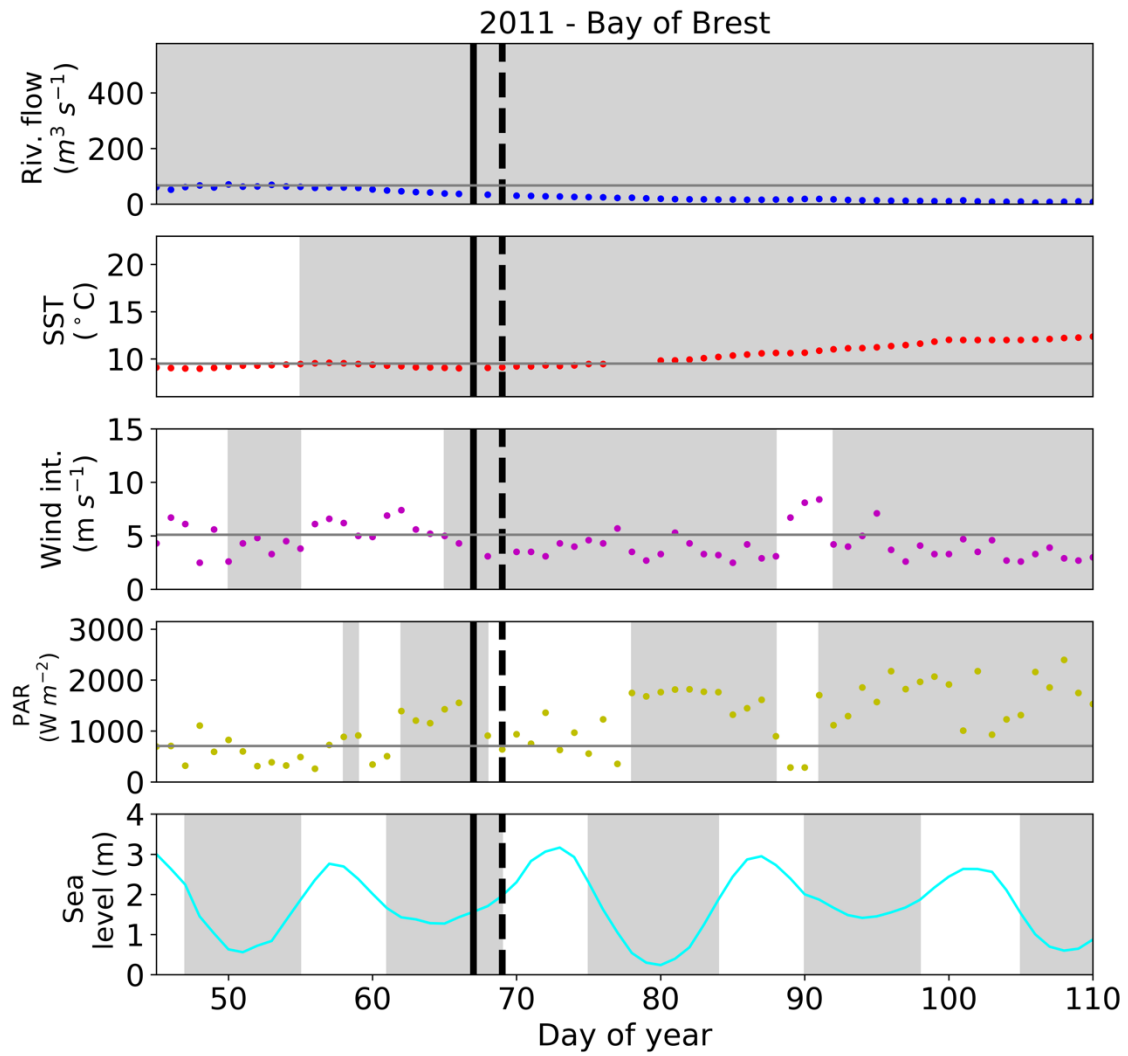


Figure 6: Changes in the IGP date in (a) the Bay of Brest and (b) the Bay of Vilaine are determined with high-frequency time series (black circles), low-frequency time series (red circles) and with the model (blue circle). The dotted black line represents the date of the COAST-HF-Molit buoy deployment.

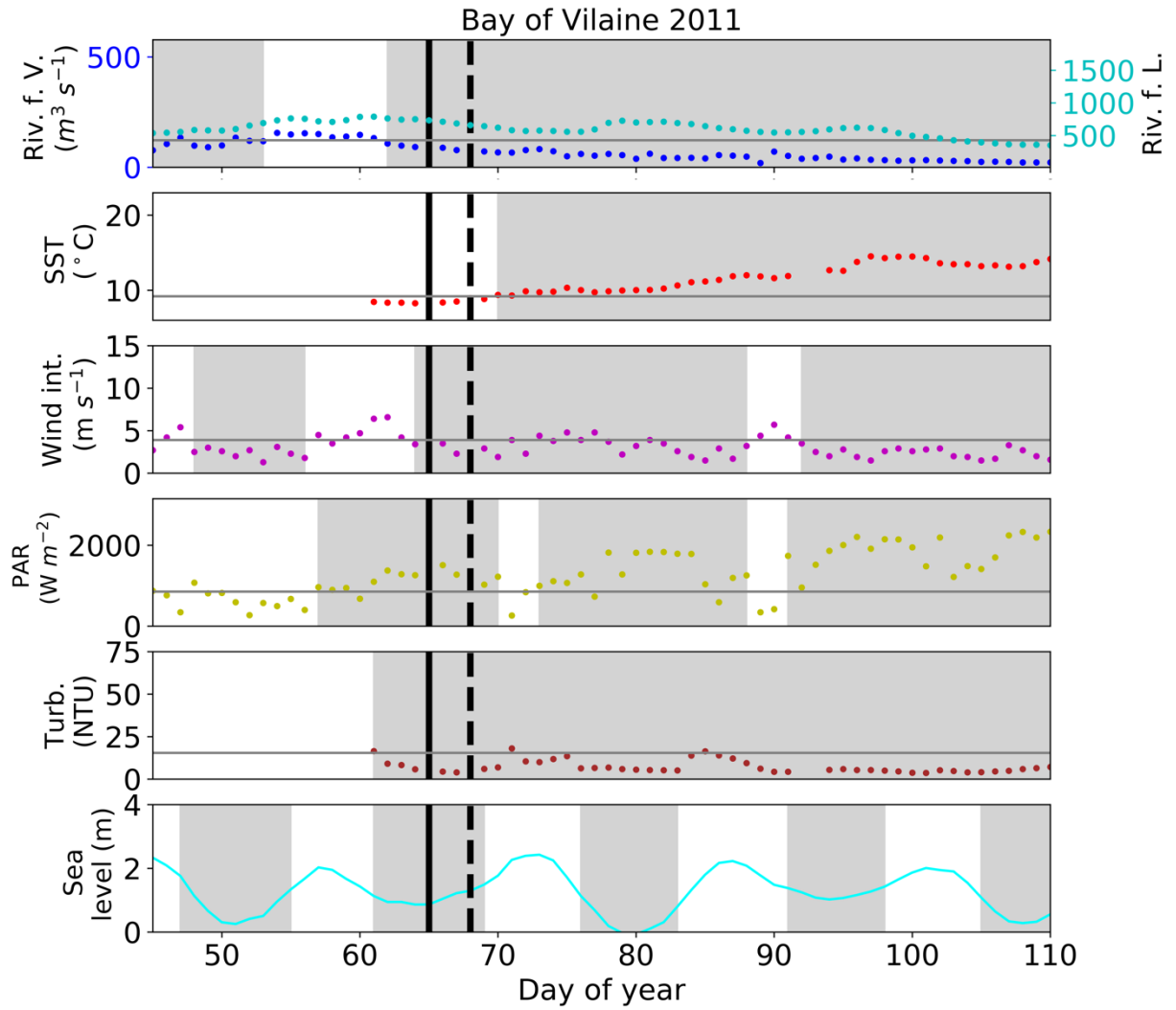
1078
 1079
 1080
 1081
 1082
 1083
 1084
 1085
 1086
 1087
 1088
 1089
 1090
 1091
 1092
 1093
 1094
 1095
 1096
 1097
 1098
 1099
 1100
 1101
 1102
 1103
 1104
 1105
 1106
 1107
 1108
 1109
 1110
 1111
 1112
 1113
 1114
 1115
 1116
 1117
 1118
 1119
 1120
 1121
 1122
 1123
 1124
 1125
 1126

1127 (a)



1128
1129
1130
1131
1132
1133
1134
1135
1136
1137
1138
1139
1140
1141
1142
1143
1144
1145
1146
1147
1148
1149
1150

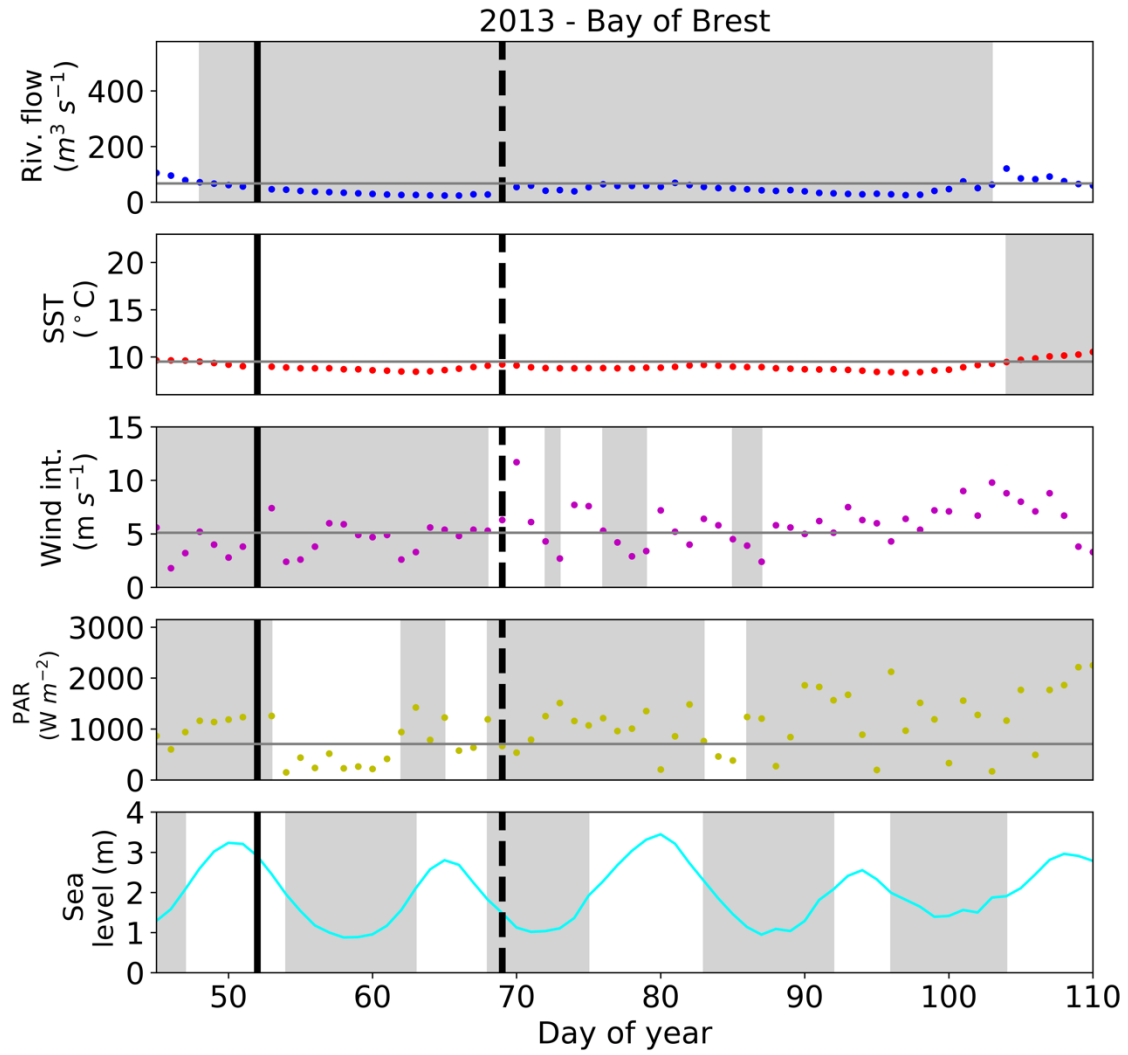
1151 (b)



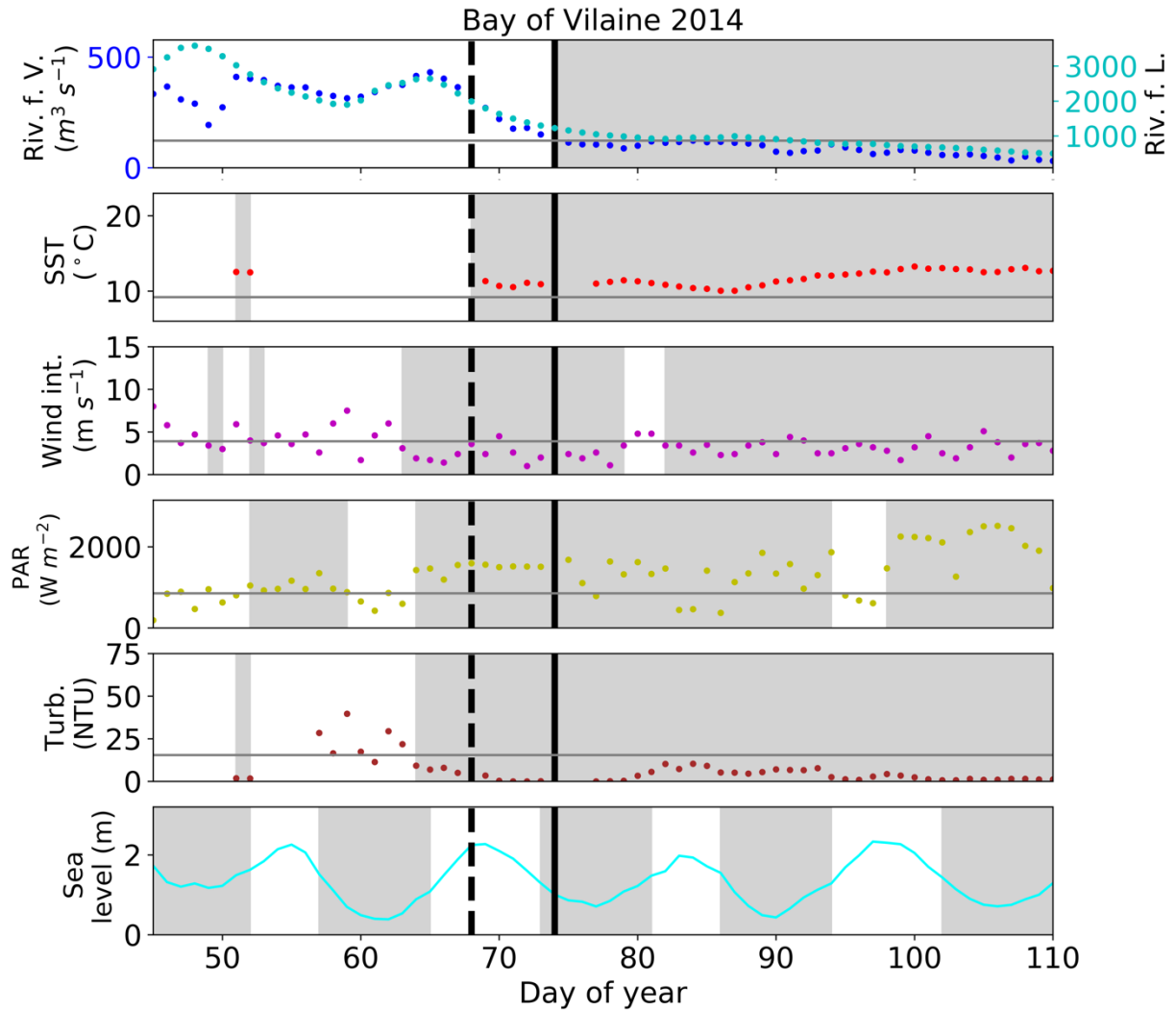
1152
1153
1154
1155
1156
1157
1158
1159
1160
1161
1162
1163
1164
1165
1166
1167
1168
1169
1170
1171
1172
1173
1174

1175
1176
1177

(c)



1178
1179
1180
1181
1182
1183
1184
1185
1186
1187
1188
1189
1190
1191
1192
1193
1194
1195
1196
1197
1198



1200
 1201
 1202
 1203
 1204
 1205
 1206
 1207
 1208
 1209
 1210

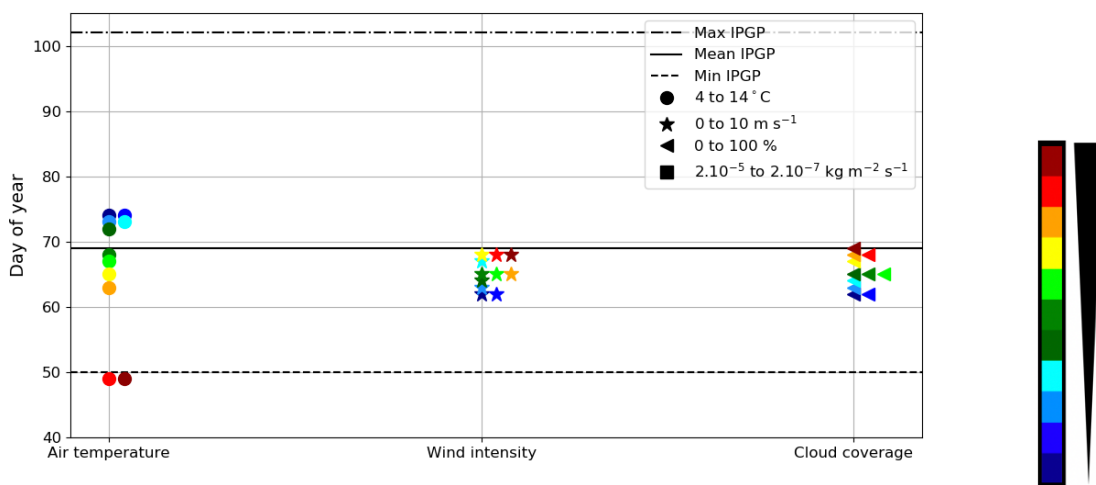
Figure 7: IPGP dates and environmental drivers: flow of the Aulne, Vilaine and Loire rivers, Sea Surface Temperature, wind intensity, PAR, turbidity and sea level at high tide. Illustrations in 2011 for a mean IPGP date in (a) the Bay of Brest and (b) the Bay of Vilaine; in 2013 for an early IPGP date in (c) the Bay of Brest; in 2014 for a late IPGP date in (d) the Bay of Vilaine. The mean IPGP date of each bay is represented by a dotted black line and the IPGP date of the year is represented by a straight black line. Thresholds of each environmental driver are represented by grey vertical lines corresponding to the mean conditions calculated 30 days around the IPGP date. Grey areas are time periods favorable to IPGP.

	Bay of Brest (2001-2019)	Bay of Vilaine (2011-2019)
	<i>Min - Median - Max</i>	<i>Min - Median - Max</i>
River flow (m ³ s ⁻¹)	13 - 46 - 100	36 - 96 - 205
SST (°C)	8 - 10 - 12	8 - 10 - 11
Wind intensity (m s ⁻¹)	1 - 3 - 6	1 - 3 - 4
PAR (W m ⁻²)	915 - 1373 - 2220	814 - 1341 - 1939
Turbidity (NTU)	1 - 7 - 21	0 - 7 - 22
Sea level (m)	0.5 - 1.6 - 2.9	0.6 - 0.9 - 1.6
PO₄ (μmol/L)	0.1 - 0.4 - 0.6	0.1 - 0.8 - 1.4
DIN (μmol/L)	8 - 20 - 38	25 - 57 - 244
Si(OH)₄ (μmol/L)	4 - 8 - 16	8 - 38 - 112

Table 4: Characteristics of environmental drivers at the date of IPGP except for nutrients from January to March in the Bay of Brest and in the Bay of Vilaine.

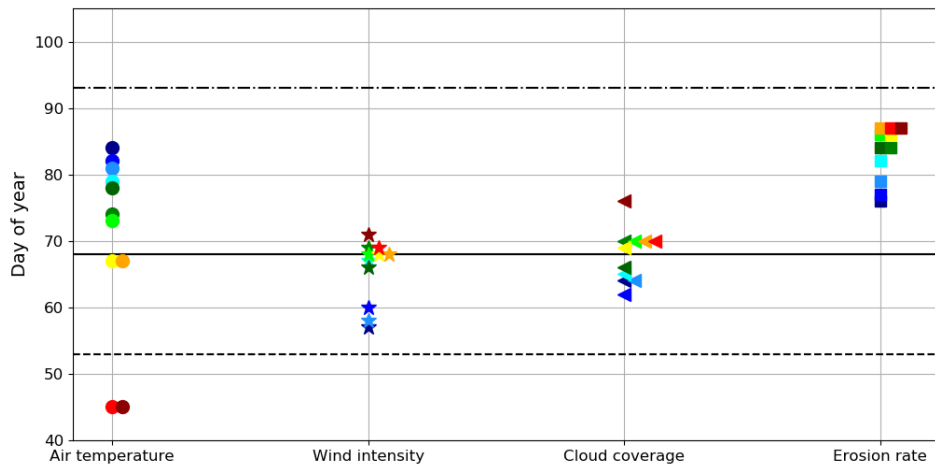
1211
1212
1213
1214
1215
1216
1217
1218

(a)



1219
1220
1221

(b)



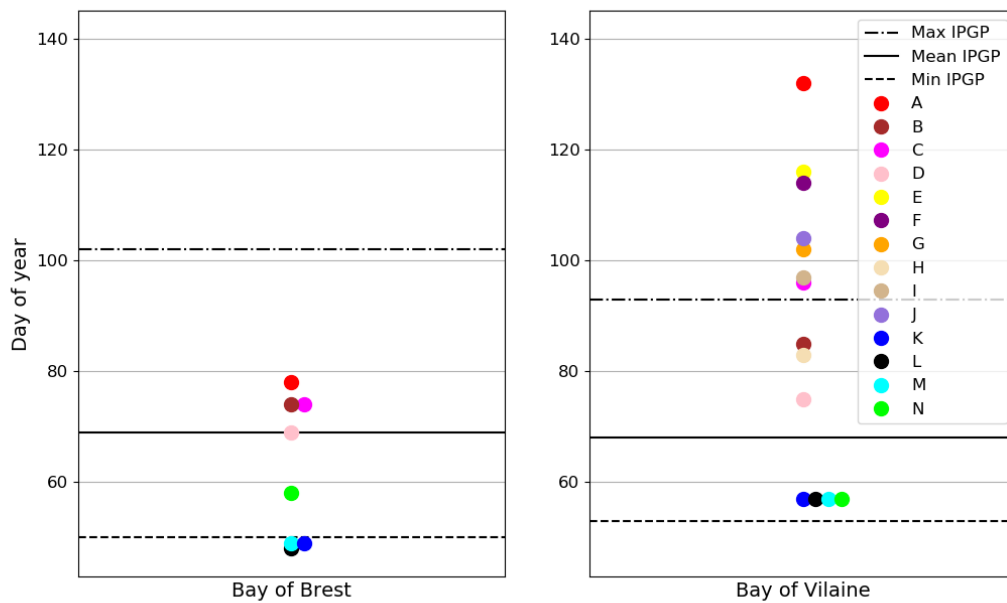
1222
1223
1224
1225
1226
1227
1228
1229

Figure 8: Impact of the variation of environmental drivers on the date of IPGP in (a) the Bay of Brest and (b) the Bay of Vilaine. Steps of: 1°C for the air temperature, 1 m s⁻¹ for the wind intensity, 10 % for the cloud coverage and 0.0000036 kg m⁻² s⁻¹ for the erosion rate equivalent to a variation of suspended matter between 0.02 and 0.08 mg L⁻¹ at IPGP.

Experiment	Air temperature (°C)	Wind intensity (m s ⁻¹)	Cloud coverage (%)	Erosion rate (kg m ⁻² s ⁻¹)	Simulated IPGP Bay of Brest (days)	Simulated IPGP Bay of Vilaine (days)
1	4	3	70	2.10 ⁻⁶	+5	+16
2	14	3	70	2.10 ⁻⁶	-20	-23
3	10	0	70	2.10 ⁻⁶	-1	-11
4	10	10	70	2.10 ⁻⁶	-7	+3
5	10	3	0	2.10 ⁻⁶	=	-4
6	10	3	100	2.10 ⁻⁶	-7	+8
7	10	3	70	2.10 ⁻⁷		+8
8	10	3	70	2.10 ⁻⁵		+19
A	4	10	100	2.10 ⁻⁵	+9	+64
B	4	10	70	2.10 ⁻⁶	+5	+17
C	4	3	100	2.10 ⁻⁶	+5	+28
D	10	10	100	2.10 ⁻⁶	=	+6
E	4	10	70	2.10 ⁻⁵		+48
F	4	3	100	2.10 ⁻⁵		+46
G	10	10	100	2.10 ⁻⁵		+34
H	10	3	100	2.10 ⁻⁵		+19
I	10	10	70	2.10 ⁻⁵		+29
J	4	3	70	2.10 ⁻⁵		+36
K	14	0	0	2.10 ⁻⁷	-20	-11
L	14	0	70	2.10 ⁻⁷	-21	-11
M	14	3	0	2.10 ⁻⁷	-20	-11
N	10	0	0	2.10 ⁻⁷	-11	-11

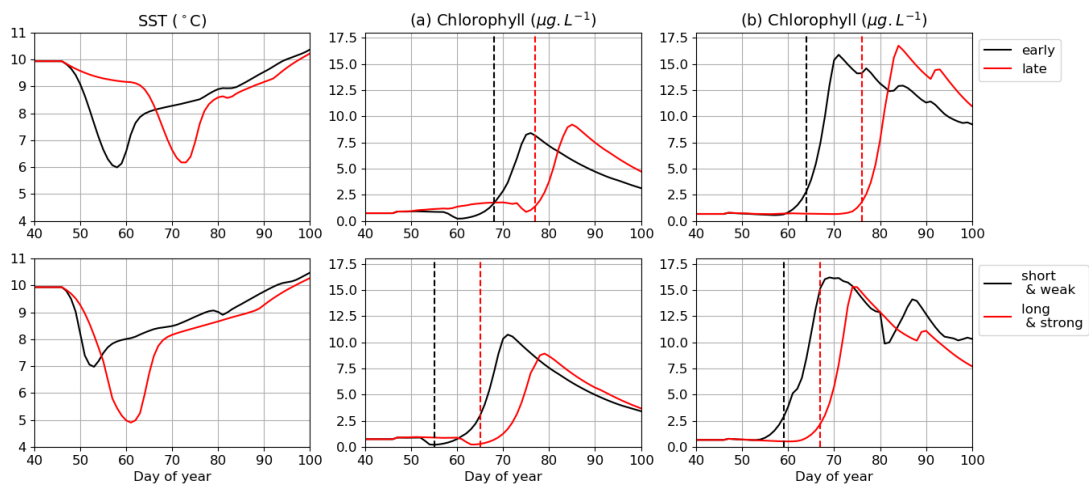
1230
1231
1232
1233

Table 5: Assumptions are explored in the 1DV model for environmental parameters independently (1-8) and with combined effect (A-N) with the modified values (grey background) and text in bold for the Bay of Brest only (+ for later IPGP, - for earlier IPGP, = for equal IPGP) with IPGP equal the mean observed IPGP of day 68.



1234
1235
1236
1237

Figure 9: Influence of combined environmental parameters for the MARS-1DV model in both bays (Bay of Brest - left and Bay of Vilaine - right) with detailed experiments in Table 2.



1238

1239
1240
1241
1242
1243
1244
1245
1246
1247
1248

Figure 10: Impact of cold spells on the IPGP date simulated in (a) the Bay of Brest and (b) the Bay of Vilaine. Four conditions of cold spells are explored: an early (mid-February), a late (end of February), a short (8 days) and a long (20 days). The IPGP dates are represented by dotted lines.